

Supporting Information

For

Solution and Solid-State Emission Toggling of a Photochromic

Hydrazone

Baihao Shao,^{†,#} Massimo Baroncini,^{‡,§,#} Hai Qian,^{†,#} Laura Bussotti,^{||,⊥} Mariangela Di Donato,^{||,⊥}
Alberto Credi,^{‡,§,*} Ivan Arahamian^{†,*}

These authors contributed equally to this work

[†] Department of Chemistry, Dartmouth College, Hanover, New Hampshire, 03755, USA

[‡] Center for Light Activated Nanostructures (CLAN), Università di Bologna and Consiglio Nazionale delle Ricerche, via Gobetti 101, 40129 Bologna, Italy

[§] Dipartimento di Scienze e Tecnologie Agro-alimentari, Università di Bologna, viale Fanin 50, 40127 Bologna, Italy

^{//} LENS – European Laboratory for Non-linear Spectroscopy, via N. Carrara 1, 50019 Sesto Fiorentino (FI), Italy

[⊥] INO - Istituto Nazionale di Ottica, Largo Enrico Fermi 6, 50125 Firenze, Italy

E-mail: ivan.aprahamian@dartmouth.edu
alberto.credi@unibo.it

Table of Contents

1. Materials and Methods	S3
2. Synthesis	S6
3. NMR Characterization	S9
4. Photoisomerization Studies in Solution	S16
5. Photoisomerization Studies in the Solid State	S22
6. Photoisomerization Quantum Yield	S23
7. Fluorescence Property Studies	S27
8. Kinetic Studies	S34
9. Crystallography	S39
10. Writing in Solution	S43
11. Solid-State Imaging	S47
12. Two-photon Excitation Experiments	S52
13. References	S55

1 Materials and Methods

All reagents and starting materials were purchased from commercial vendors and used as supplied unless otherwise indicated. Fetal bovine serum was stored under -20°C before usage. All experiments were conducted under air unless otherwise noted. Compounds were purified by column chromatography using silica gel (SiliCycle[®], 60 Å, 230-400 mesh) as stationary phase and solvents mixtures used during chromatography were reported as volume ratios unless otherwise noted. Deuterated solvents were purchased from Cambridge Isotope Laboratories, Inc. and used as received. ^1H NMR, ^{13}C NMR and 2D NMR spectra were recorded on a 500 or 600 MHz NMR spectrometer, with working frequencies of 500.13 or 600.13 MHz for ^1H nuclei, and 125.8 or 150.9 MHz for ^{13}C nuclei, respectively. Chemical shifts are quoted in ppm relative to tetramethylsilane (TMS), using the residual solvent peak as the reference standard. ESI mass spectra were obtained on a Shimadzu LCMS-8030 mass spectrometer. Melting points were measured on an Electrothermal Thermo Scientific IA9100X1 digital melting point instrument. UV-Vis spectra were recorded on a Shimadzu UV-1800 UV-Vis spectrophotometer.

Irradiation experiments were conducted with a stand-alone xenon arc lamp system (Model: LB-LS/30, Sutter Instrument Co.), outfitted with a SMART SHUTTER controller (Model: LB10-B/IQ, Sutter Instrument Co.) and a liquid light guide LLG/250. 340 (part number: 340HC10-25), and 442 (part number: 442F5X10-25) nm light filters, purchased from Andover Corporation, were used in the irradiation experiments.

Stock solutions were prepared by dissolving appropriate amounts of **1** in toluene, followed by stirring to ensure sample homogeneity. The desired concentration was reached by consecutive dilutions. The fluorescence spectra were collected immediately after the sample was prepared. A Photon Technology International QuantaMaster 4 spectrofluorometer outfitted with a LPS-100 lamp power supply and Xenon arc lamp housing, ASOC-10 electronics interface, MD-4 motor driver control, and a model 914D photomultiplier detector system was used to collect fluorescence spectra. Data were acquired with a step size of 0.5 nm, an integration time of 0.1 s, and slit widths

of 5 nm.

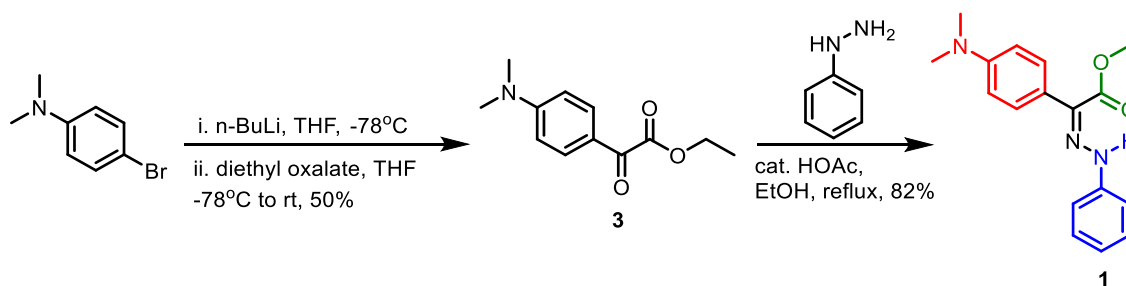
For fluorescence lifetime measurements, toluene solutions of **1** (5×10^{-6} M) were used. Fluorescence lifetime was determined by time-correlated single photon-counting (TCSPC) using a Photon Technology International QuantaMaster 4 spectrofluorometer integrated with Deltadiode-375L diode laser ($\lambda_{\text{ex}} = 373$ nm, < 70 ps pulse width) as the excitation source. The fluorescence decays were detected using a fast PPD-850 detector. In all cases, decays were recorded until peak counts reached 10,000. The decay traces were analyzed by the one-exponential fitting method using Felix data analysis from Horiba Scientific Ltd. Quantum yields of **1-Z** in toluene and serum buffer, and its powder were measured, using Horiba model 914D photomultiplier detector system with a calibrated integrating sphere system.

For the photoisomerization studies in the solid state, absorption spectra were recorded at room temperature (ca. 25°C) with a Perkin Elmer Lambda 750 spectrophotometer. Luminescence spectra were recorded at 25°C on an Edinburgh FLS 980 spectrofluorimeter. Polarizing optical micrographs were taken using a Nikon Eclipse 80i polarizing optical microscope. Photochemical experiments were performed at room temperature on films deposited on a quartz plate by drop casting from a dichloromethane solution (1 mg in 1 mL). The light source used for irradiation was a CoolLED pE-300. The selection of the desired irradiation wavelength (360 or 450 nm) was accomplished by the use of an appropriate interference filter.

The excitation source for all the two-photon experiments was provided by a femtosecond Ti-sapphire oscillator (Tsunami, Spectra Physics) and regenerative amplifier laser system (BMI Alpha 1000) producing 430 mW, 100 fs pulses tunable in the 750-810 nm range at 1KHz repetition rate. Two-photon induced fluorescence of **1-Z** was recorded using an optical fiber coupled to a portable spectrometer (Ocean Optics USB-650). Data were acquired using 1s integration time. The sample was contained in a 1 cm quartz cuvette and excited at 800 nm. Two BG40 bandpass filters were placed in series before the detector to suppress the residual pump light. One-photon induced fluorescence was recorded for comparison using the same laser source and detection system.

Excitation pulses at 400 nm were produced by second harmonic generation of the fundamental 800 nm laser radiation using a 2 mm thick BBO crystal.

2 Synthesis



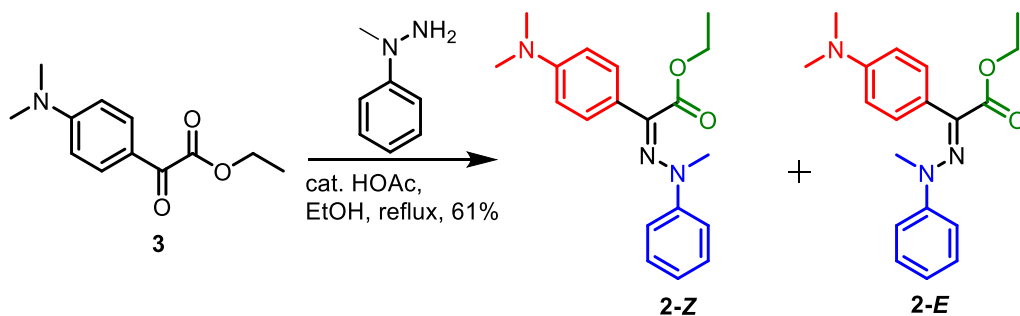
Scheme S1. Synthesis of 1.

3: This compound was synthesized using a reported procedure,^{S1} and its identity was confirmed by comparing the obtained ¹H NMR spectrum with the published one. ¹H NMR (500 MHz, CDCl₃) δ 7.90 (d, *J* = 9.2 Hz, 2H, Ar-H), 6.66 (d, *J* = 9.2 Hz, 2H, Ar-H), 4.41 (q, *J* = 7.1 Hz, 2H, CH₂), 3.10 (s, 6H, N(CH₃)₂), 1.41 (t, *J* = 7.2 Hz, 3H, CH₃) ppm.

1: Phenylhydrazine (0.1 mL, 1 mmol) and several drops of acetic acid were added to a 50 mL flask containing **3** (0.2 g, 0.9 mmol) dissolved in 30 mL of ethanol. The reaction mixture was then refluxed for 3 hours under nitrogen. After cooling to room temperature, 20 mL of water was added to afford a yellow precipitate, which was collected by filtration and washed with water. The crude residue was subjected to column chromatography using 15:1 hexanes/ethyl acetate as eluent to give hydrazone **1-Z** as a yellow solid. Yield: 0.23 g (82%). **1-Z:** ¹H NMR (500 MHz, CD₃CN) δ 11.77 (s, 1H, NH), 7.52 (d, *J* = 9.0 Hz, 2H, Ar-CH), 7.34 – 7.29 (m, 2H, Ar-CH), 7.26 (d, *J* = 7.5 Hz, 2H, Ar-CH), 6.95 (t, *J* = 7.2 Hz, 1H, Ar-CH), 6.74 (d, *J* = 9.0 Hz, 2H, Ar-CH), 4.34 (q, *J* = 7.1 Hz, 2H, CH₂), 2.96 (s, 6H, 2 × NCH₃), 1.32 (t, *J* = 7.1 Hz, 3H, CH₃); ¹³C-NMR (151 MHz, CD₃CN) δ 164.28 (C=O), 151.02, 144.5, 130.65, 129.90, 129.78, 122.14, 114.22, 112.88, 112.18, 61.64, 40.23, 14.00; Mp: 94.9°C –95.2°C; HRMS (ES⁺) *m/z*: [M+H]⁺ calcd 312.1712, found 312.1707. **1-E:** ¹H NMR (600 MHz, CD₃CN) δ 8.66 (s, 1H, NH), 7.29 (t, *J* = 8.6 Hz, 2H, Ar-CH), 7.22 (d, *J* = 8.8 Hz, 2H, Ar-CH), 7.17 (d, *J* = 8.8 Hz, 2H, Ar-CH), 6.94 (t, *J* = 7.4 Hz, 1H, Ar-CH), 6.88 (d, 2H, *J* = 8.9 Hz, Ar-CH), 4.26 (q, *J* = 7.1 Hz, 2H, CH₂), 3.03 (s, 6H, 2 × NCH₃), 1.32 (t, *J* = 7.1

Hz, 3H, CH₃); ¹³C-NMR (151 MHz, CD₃CN) δ 164.54 (C=O), 150.73, 143.51, 135.00, 129.74, 128.98, 128.85, 120.98, 113.37, 111.97, 60.23, 39.14, 13.37 ppm.

Hydrazone **1** in CD₃CN exhibits a characteristic N-H proton signal at δ = 11.8 ppm, indicating that this proton is H-bonded with the carbonyl group, i.e., the compound adopts the *Z* configuration. As a matter of fact, the compound exclusively adopts the *Z* configuration (>99%) in solution because no other signals can be detected in the ¹H NMR spectrum. The single crystal structure of **1** also shows the presence of an intramolecular H-bond between N-H proton and the carbonyl oxygen (N-H⋯O=C, 2.626(3) Å, 132.54°). This result indicates that the switch adopts the *Z* configuration in the solid-state as well.



Scheme S2. Synthesis of control compound **2**.

2: 1-methyl-1-phenylhydrazine (0.16 mL, 1.27 mmol) and several drops of acetic acid were added to a 50 mL flask containing **3** (200 mg, 0.90 mmol) dissolved in 10 mL of ethanol. The mixture was refluxed for 6 hours under nitrogen. After cooling to room temperature, 10 mL of water was added, and then solution was extracted with methylene chloride (2 × 20 mL). The organic phase was washed with brine (30 mL) and dried over anhydrous Na₂SO₄. Solvent was removed under reduced pressure, and the residue was subjected to column chromatography using 20:1 hexanes/ethyl acetate to afford **2-Z** as a yellow solid, and a 6:1 mixture of **2-E** and **2-Z** (40 mg, 14%). **2-Z:** Yield: 140 mg (47%); ¹H-NMR (600 MHz, CD₃CN) δ 7.58 (d, *J* = 9.0 Hz, 2H, Ar-CH),

7.27 (t, $J = 8.5$ Hz, 2H, Ar-CH), 7.03 (d, $J = 8.0$ Hz, 2H, Ar-CH), 6.91 (t, $J = 7.3$ Hz, 1H, Ar-CH), 6.76 (d, $J = 9.0$ Hz, 2H, Ar-CH), 4.32 (q, $J = 7.1$ Hz, 2H, CH₂), 3.13 (s, 3H, NCH₃), 3.01 (s, 6H, 2 × NCH₃), 1.25 (t, $J = 7.1$ Hz, 3H, CH₃); ¹³C NMR (151 MHz, CD₃CN) δ 166.78 (C=O), 158.87, 153.06, 151.36, 129.23, 128.84, 121.13, 119.84, 116.34, 112.28, 61.87, 41.77, 39.93, 14.00 ppm; Mp: 85.1°C –86.0°C; HRMS (ES+) m/z : [M+H]⁺ calcd 326.1869, found 326.1866. **2-E**: ¹H-NMR (600 MHz, CD₃CN) δ 7.39 – 7.32 (m, 4H, Ar-CH), 7.23 (d, $J = 9.0$ Hz, 2H, Ar-CH), 7.03 – 6.99 (m, 1H, Ar-CH), 6.75 (d, $J = 9.0$ Hz, 2H, Ar-CH), 4.27 (q, $J = 7.1$ Hz, 2H, CH₂), 3.02 (s, 3H, NCH₃), 3.00 (s, 6H, 2 × NCH₃), 1.33 (t, $J = 7.1$ Hz, 3H, CH₃) ppm; ¹³C NMR (151 MHz, CD₃CN) δ 166.85 (C=O), 151.20, 149.79, 137.75, 131.08, 129.44, 122.51, 122.00, 116.14, 111.60, 61.37, 40.91, 40.04, 14.27 ppm.

3 NMR Characterization

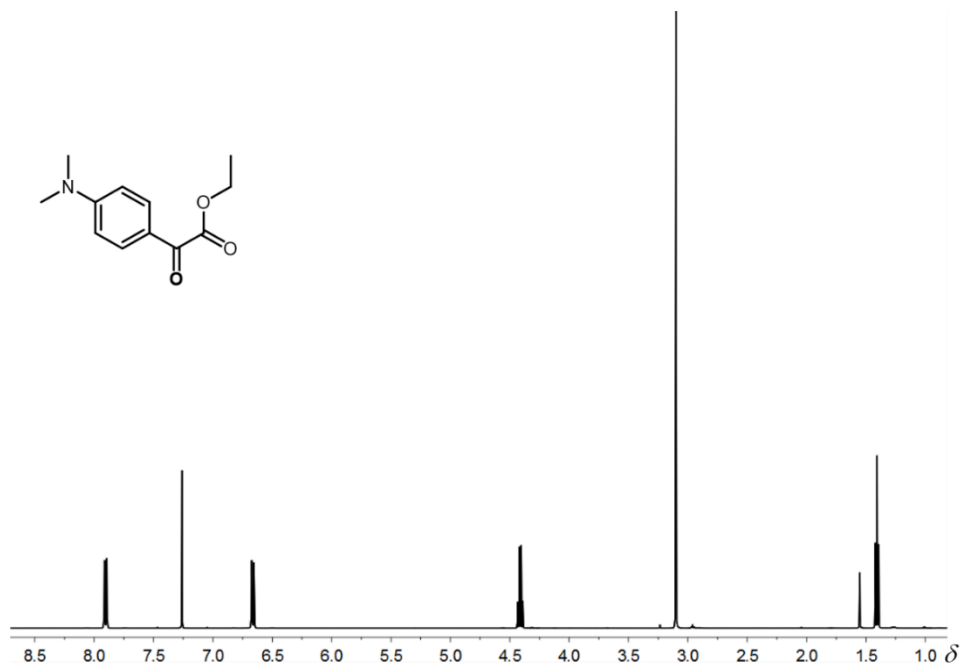


Figure S1. ¹H NMR spectrum of **3** in CD₃CN at 294 K.

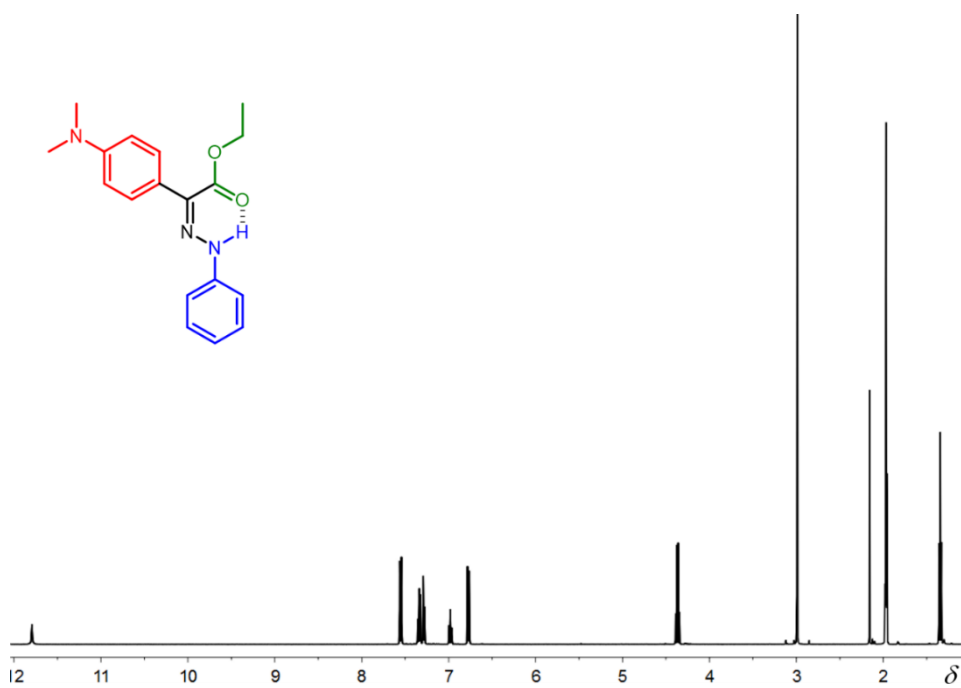


Figure S2. ¹H NMR spectrum of **1** in CD₃CN at 294 K.

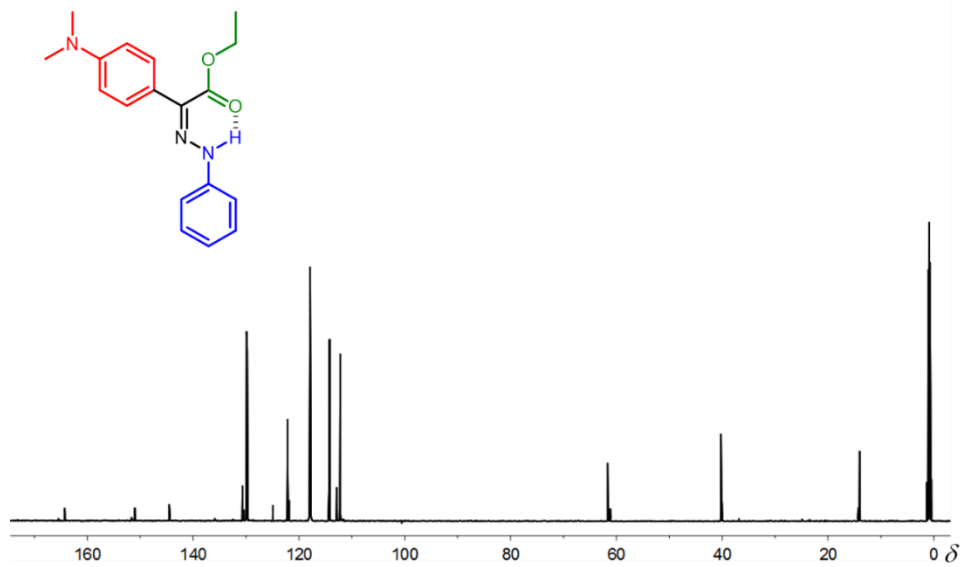


Figure S3. ^{13}C NMR spectrum of **1** in CD_3CN at 294 K.

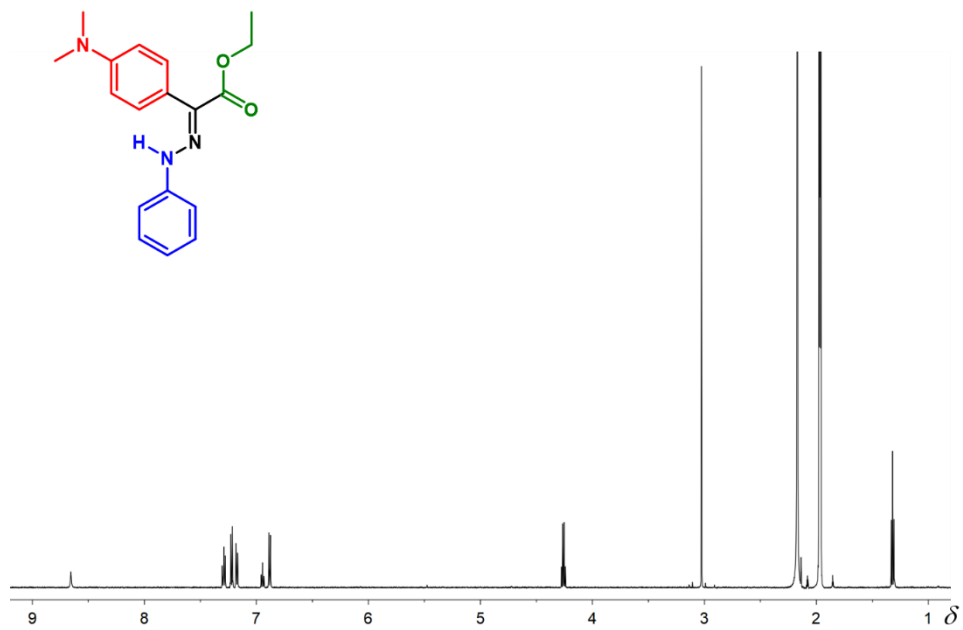


Figure S4. ^1H NMR spectrum of **1-E** in CD_3CN at 294 K.

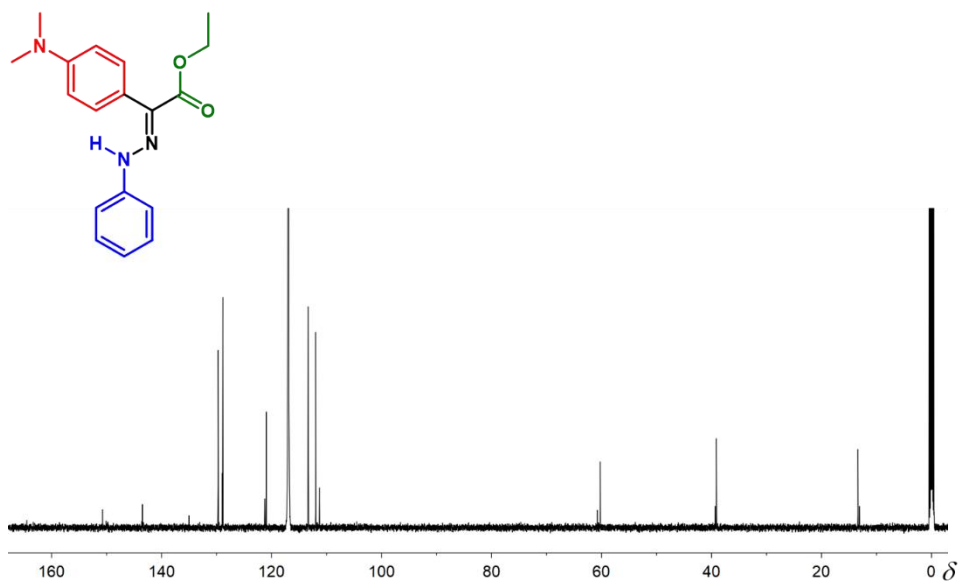


Figure S5. ¹³C NMR spectrum of **1-E** in CD₃CN at 294 K.

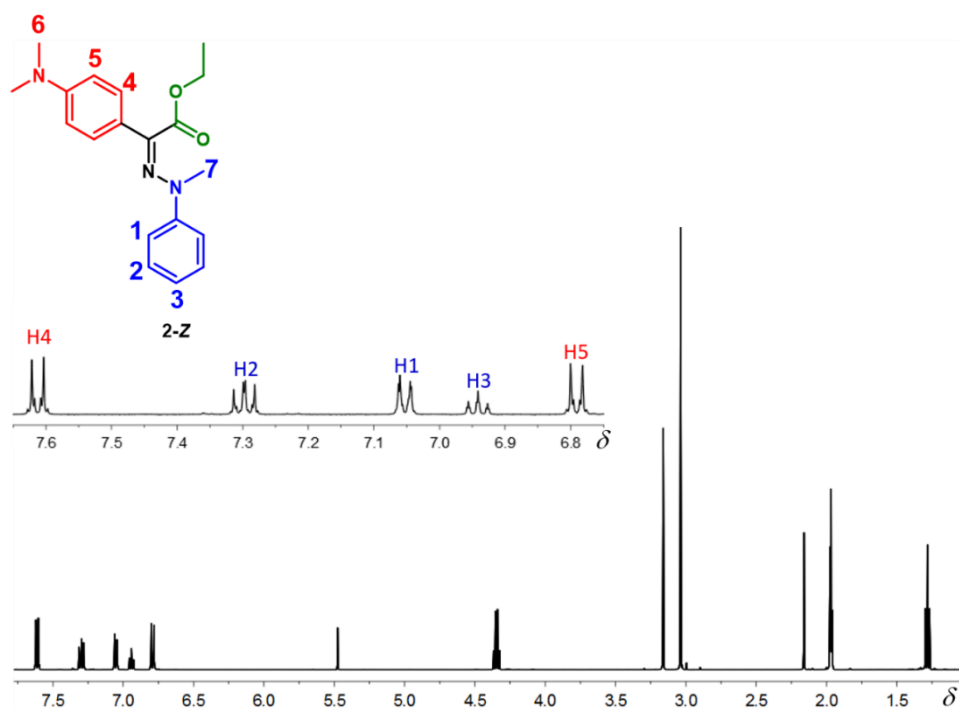


Figure S6. ¹H NMR spectrum of **2-Z** in CD₃CN at 294 K.

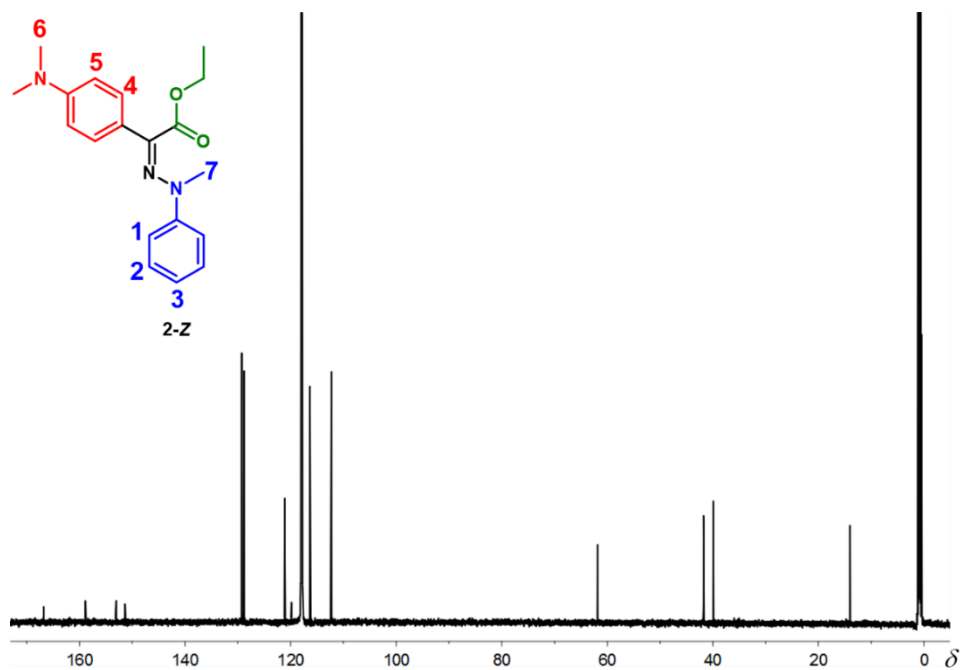


Figure S7. ¹³C NMR spectrum of 2-Z in CD₃CN at 294 K.

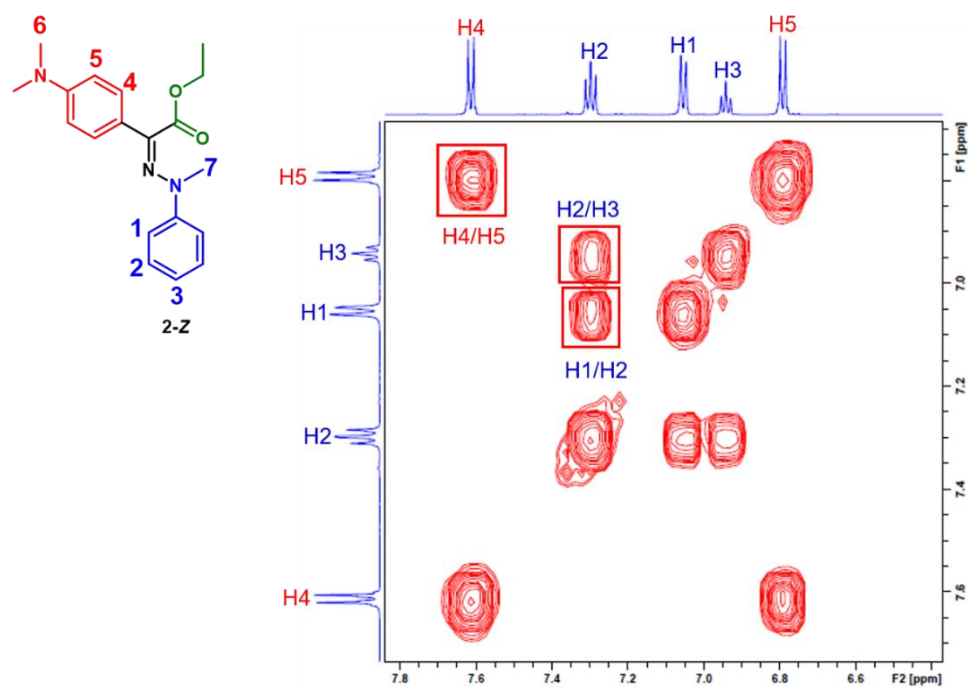


Figure S8. 2D COSY of 2-Z in CD₃CN at 294 K.

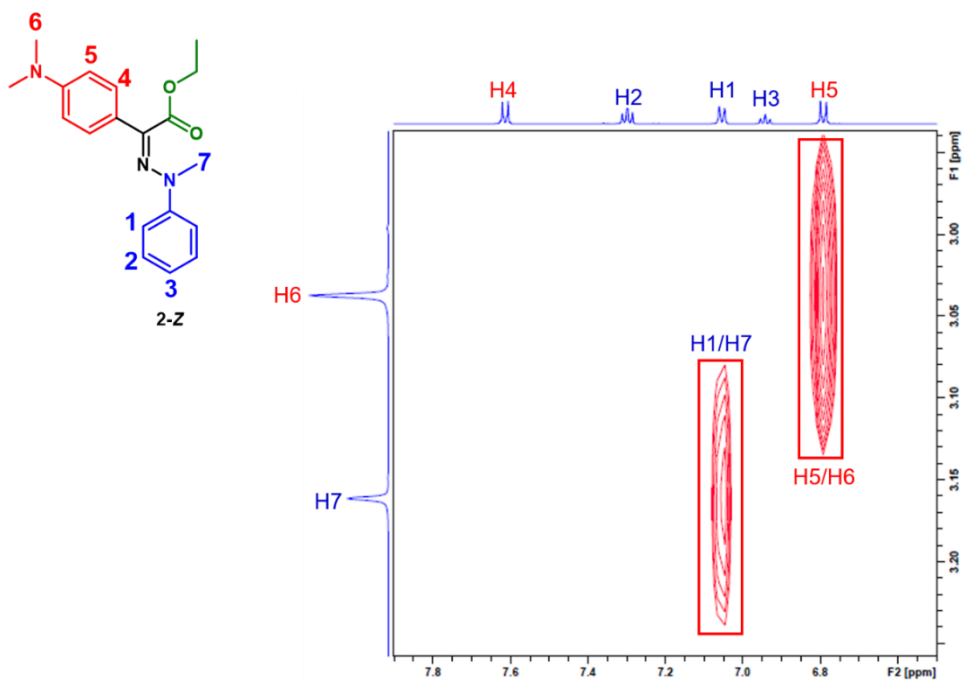


Figure S9. 2D NOESY of 2-Z in CD₃CN at 294 K.

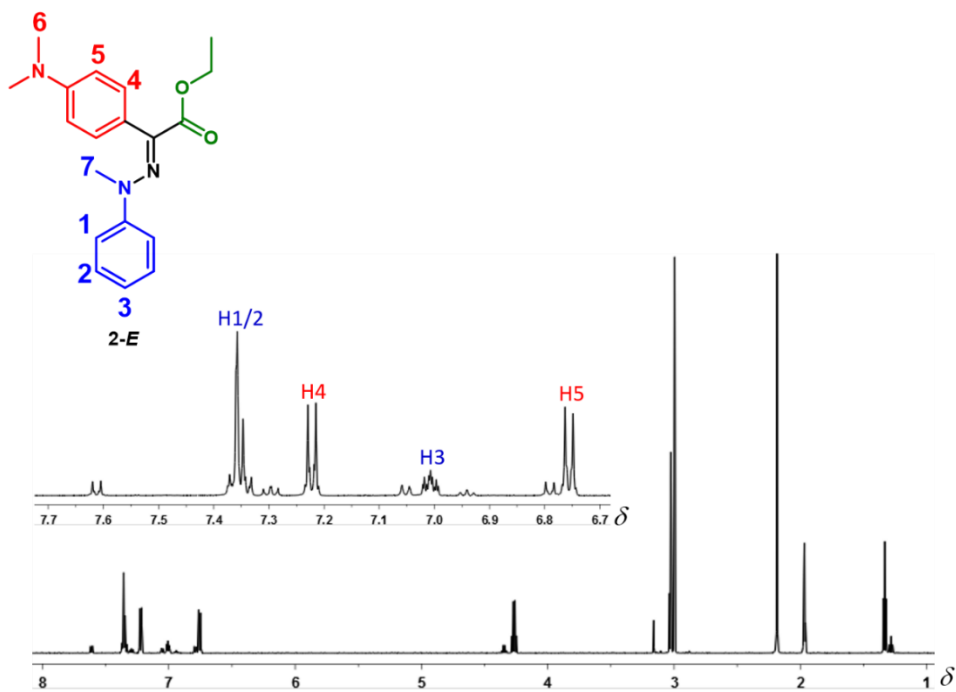


Figure S10. ¹H NMR spectrum of 2-E in CD₃CN at 294 K.

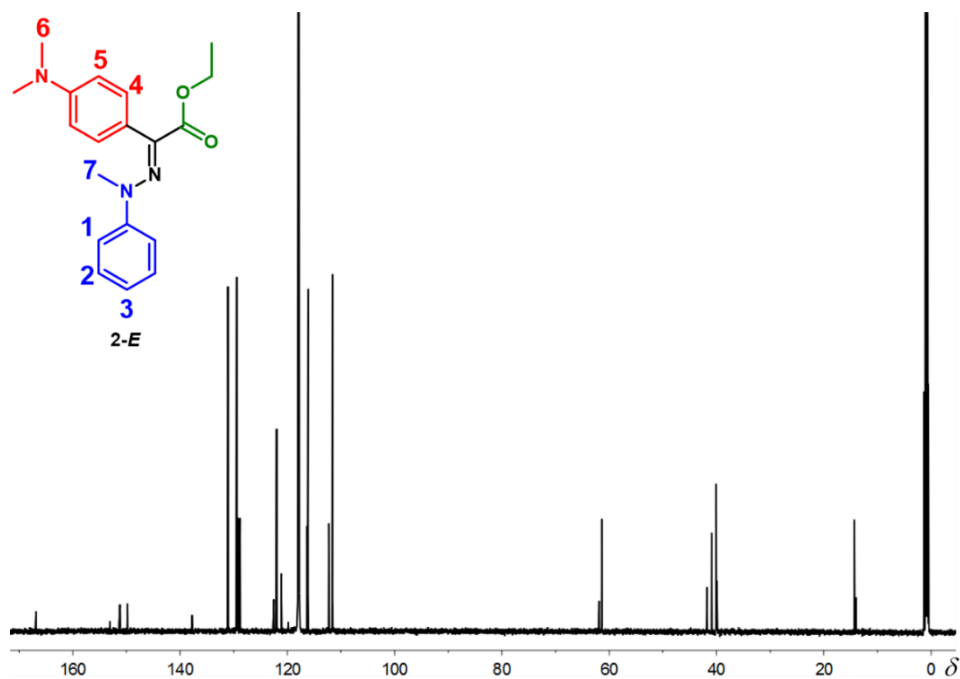


Figure S11. ^{13}C NMR spectrum of **2-E** in CD_3CN at 294 K.

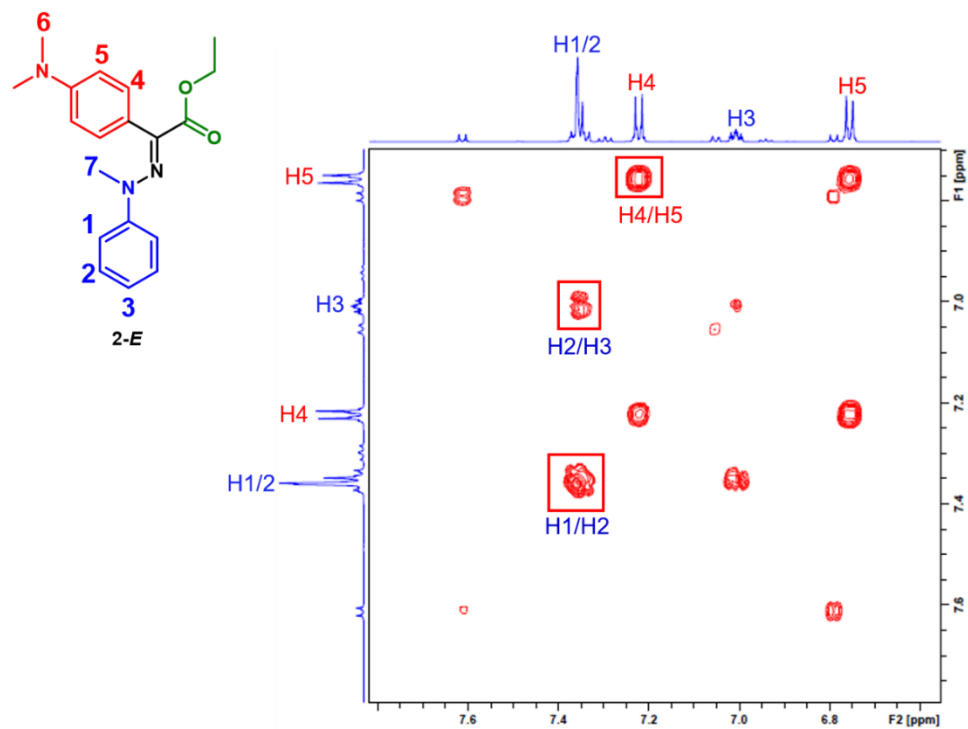


Figure S12. 2D COSY of **2-E** in CD_3CN at 294 K.

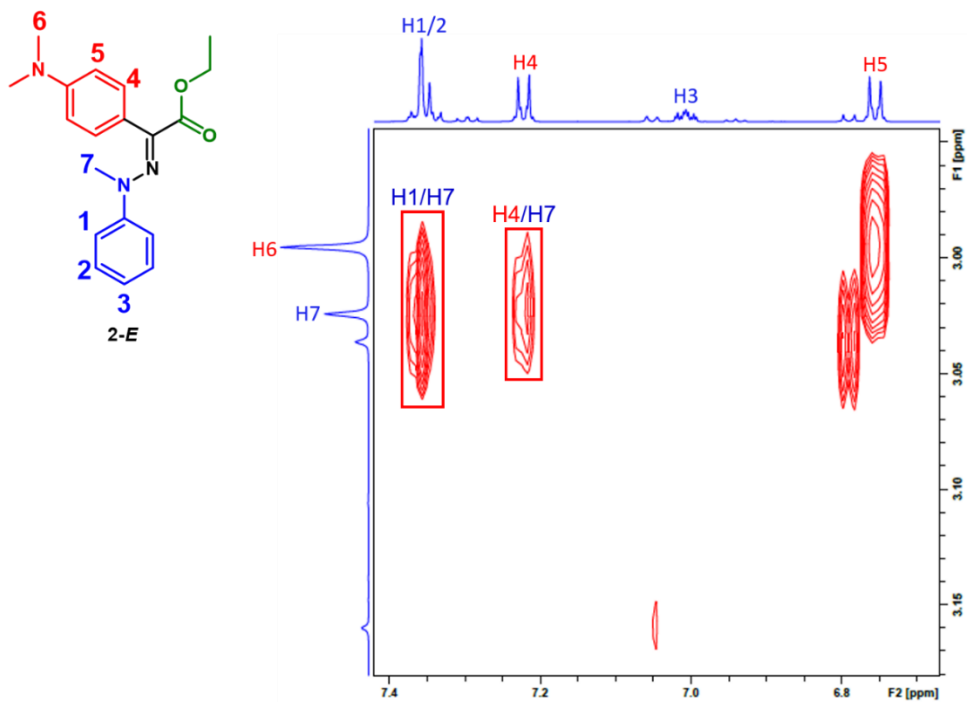


Figure S13. 2D NOESY of **2-E** in CD₃CN at 294 K.

4 Photoisomerization Studies in Solution

UV-Vis and ^1H NMR spectroscopies were employed to study the photoisomerization of the hydrazone switches. Spectrophotometric grade solvents were used for the UV/Vis absorption studies. Hydrazone switch solutions (3.0 mL, 1.0×10^{-5} M) in toluene were prepared and transferred into a 1.0 cm quartz cuvette for immediate UV/Vis absorption measurements. The solutions were irradiated with appropriate light sources, and the corresponding UV spectra were recorded. Isomerization cycles were measured by alternating irradiation wavelengths and monitoring the absorbance change at a chosen wavelength. The photostationary states (PSS) were determined upon continuous irradiation of the sample until no further isomerization was observed using ^1H NMR spectroscopy.

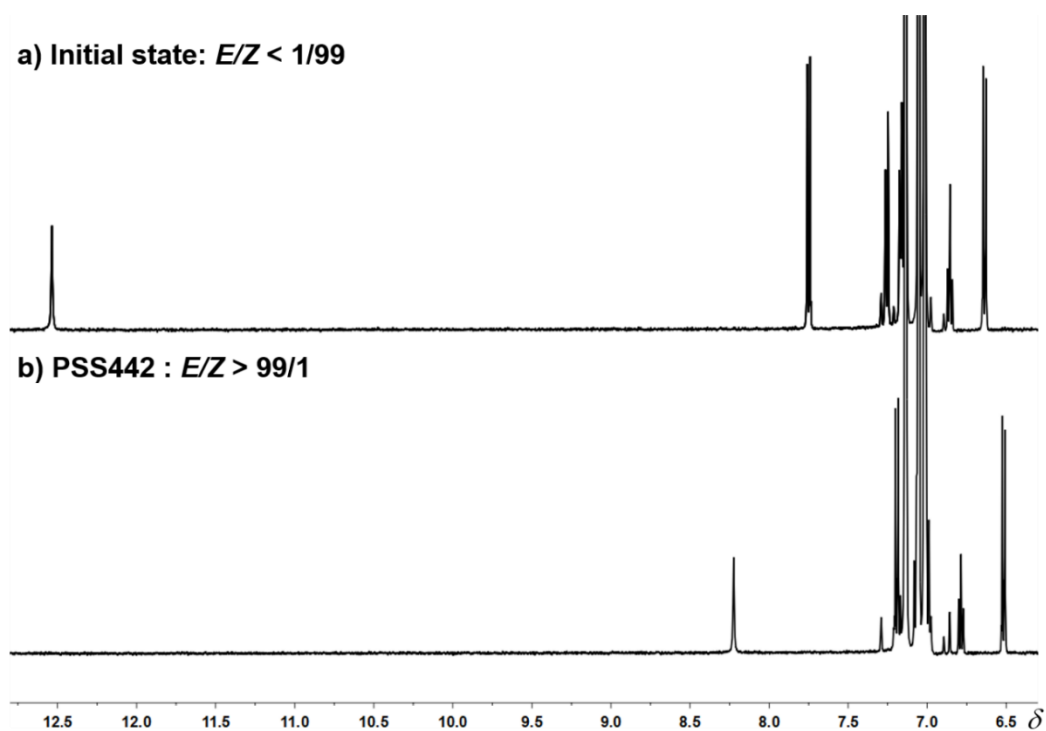


Figure S14. ^1H NMR spectra of hydrazone switch **1-Z** a) before and b) after 442 nm photo-irradiation to reach PSS in toluene- d_8 at 294 K.

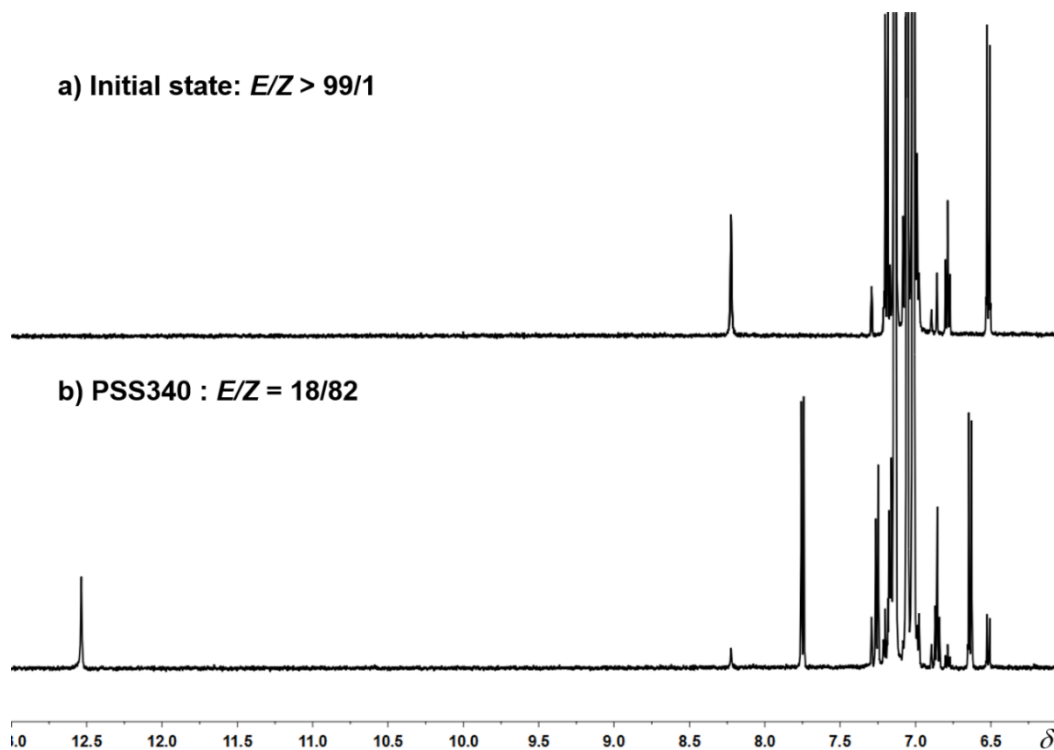


Figure S15. ^1H NMR spectra of hydrazone switch **1-E** a) before and b) after 340 nm photo-irradiation to reach PSS in toluene- d_8 at 294 K.

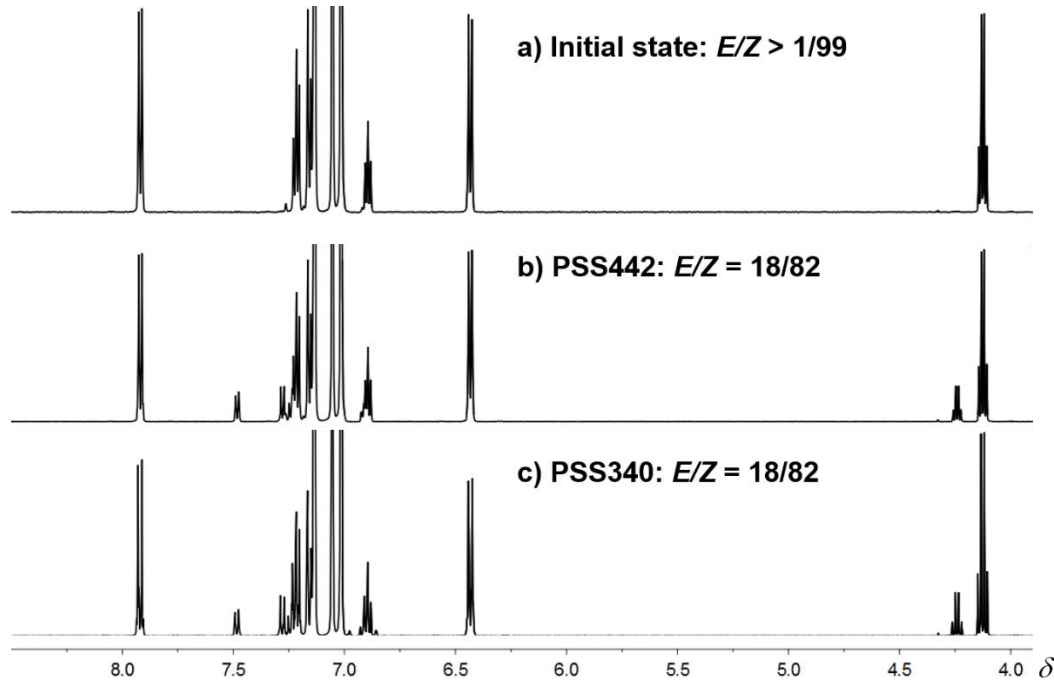


Figure S16. ^1H NMR spectra of hydrazone switch **2** a) before irradiation b) after 442 nm photo-irradiation to reach PSS in toluene- d_8 at 294 K; c) after 340 nm photo-irradiation, no back isomerization was observed at this wavelength!

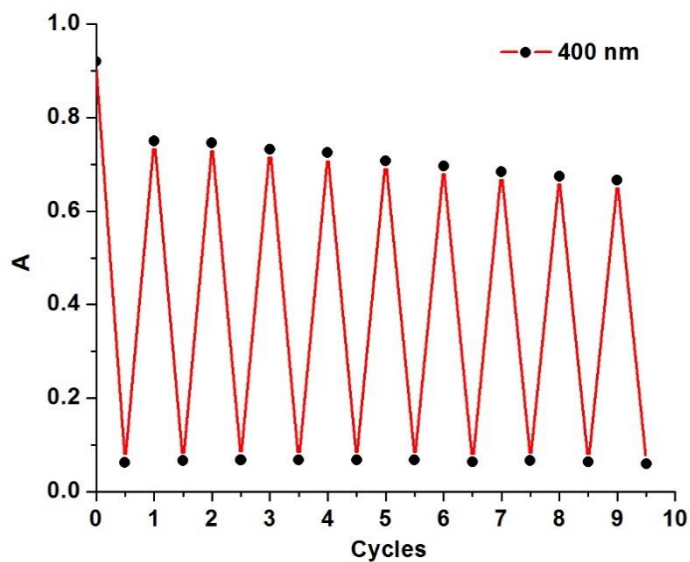


Figure S17. Switching cycles of **1** (5.0×10^{-5} M) in toluene. The absorbance change at $\lambda = 400$ nm was monitored using UV/Vis spectroscopy while alternating the irradiation wavelength between 442 and 340 nm.

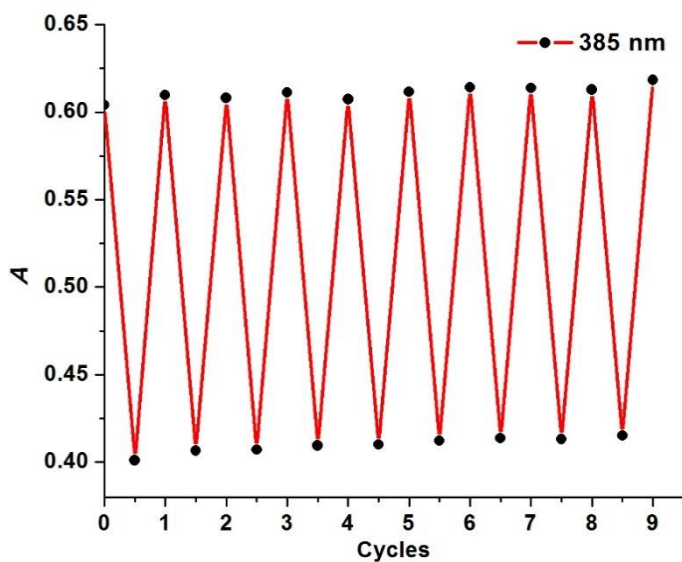


Figure S18. Switching cycles of **1** (5.0×10^{-5} M) in aqueous medium (MeOH: H₂O = 1:1). The absorbance change at $\lambda = 385$ nm was monitored using UV/Vis spectroscopy while alternating the irradiation wavelength between 442 and 340 nm.

Switching of **1** in serum buffer

A 10 mM phosphate-buffer saline (PBS) solution was prepared by dissolving 8.00g sodium chloride (NaCl), 0.20g potassium chloride (KCl), 1.44g sodium phosphate dibasic dihydrate ($\text{Na}_2\text{HPO}_4 \cdot 2\text{H}_2\text{O}$) and 0.24g potassium phosphate monobasic (K_2HPO_4) in 800 mL distilled water. 2 M HCl was used to adjust the pH to 7.4, followed by adjusting the volume to 1 L with additional distilled water. To prepare a 10% fetal bovine serum (FBS) buffer for switching studies, FBS, DMSO, and 10 mM PBS buffer were mixed at a ratio of 1:1:8. DMSO was used to solubilize the switch in the FBS buffer solution. The emission of **1-Z** is quenched in a water/DMSO solution (10% DMSO). However, it is regained in the FBS buffer. Interaction with proteins in the buffer might explain this phenomenon.

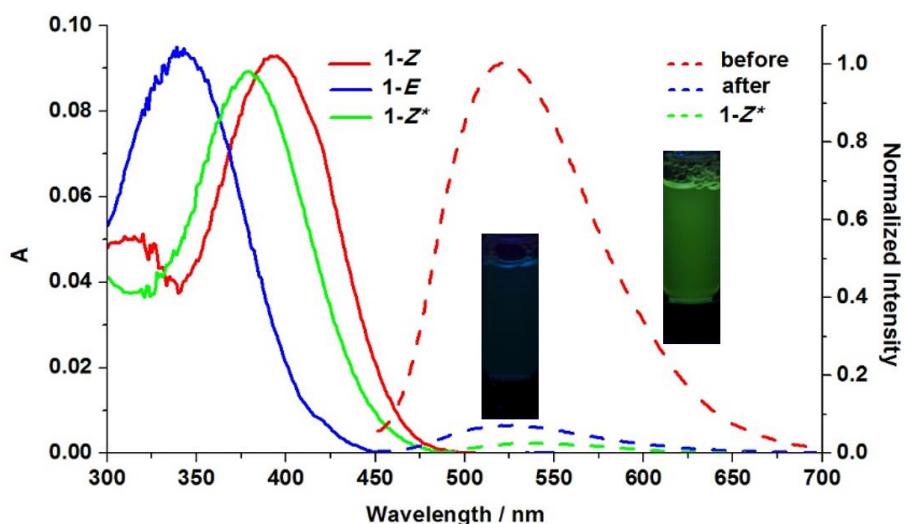


Figure S19. Solid lines: UV-Vis spectra (5.0×10^{-6} M) of **1-Z** and **1-E** in 10% FBS buffer; Dashed lines: Fluorescence emission spectra (5.0×10^{-6} M, $\lambda_{ex} = 420$ nm) of **1** in 10% FBS buffer, before irradiation (red) and after irradiation (blue); **1-Z*** refers to **1-Z** (5.0×10^{-6} M) in water (with 10% DMSO).

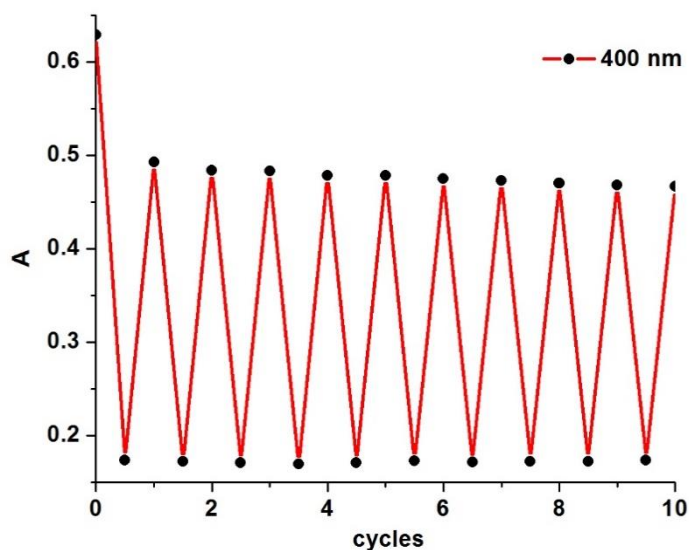


Figure S20. Switching cycles of **1** (5.0×10^{-5} M) in FBS buffer. The absorbance change at $\lambda = 400$ nm was monitored using UV/Vis spectroscopy, while alternating the irradiation wavelength between 442 and 340 nm.

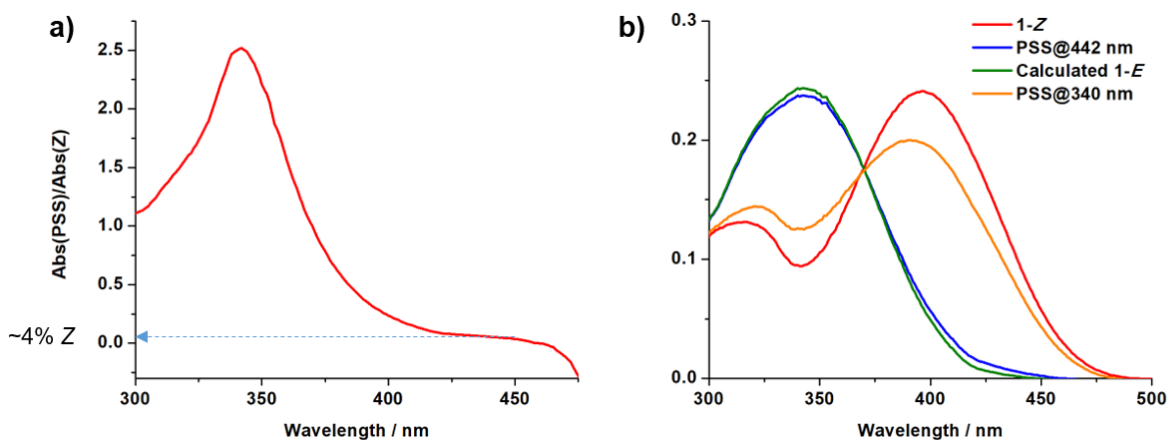


Figure S21. (a) The plot of Abs (PSS)/Abs (Z) ratio *versus* wavelength^{S2} from which the PSS of **1-E** was calculated (PSS₄₄₂ = 96%). (b) UV-Vis spectra of **1-Z** (1.0×10^{-5} M) and PSSs (442 and 340 nm) in 10% FBS buffer. The absorption spectrum of **1-E** was calculated using the equation: Abs (E) = (Abs (PSS@442 nm) - Z% \times Abs (Z)) / E%, where Z% and E% refer to the percentages of Z and E isomers at the photostationary state obtained under 442 nm light irradiation (i.e., 96% of **1-E** and 4% of **1-Z**).

The photostationary state under 340 nm light irradiation is determined by using linear equation in two unknowns: Abs (PSS@340 nm) = x \times Abs (Z) + y \times Abs (E); where x and y are the percentages of the Z and E isomers, respectively, at PSS₃₄₀. Applying two sets of absorption data (at absorption

maximum of **1-Z** (395 nm) and isosbestic point (370 nm), the PSS₃₄₀ was calculated to be composed of 76% of **1-Z**.

Titration of aqueous solution of **1-Z** with bovine serum albumin (BSA), a component of FBS, leads to enhancement of emission, indicating that the latter is providing a hydrophobic environment for **1-Z** that reinstates its emission in aqueous media.^{S3}

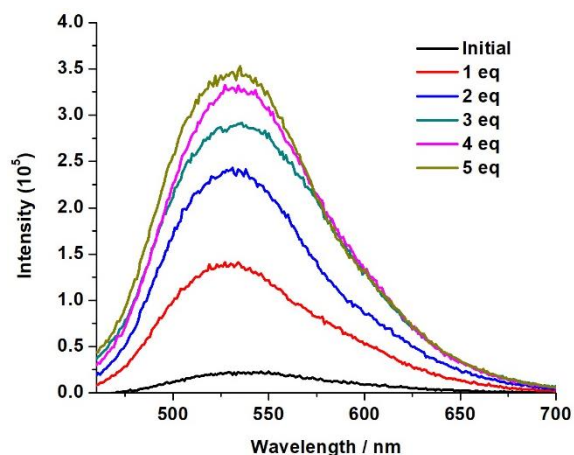


Figure S22. Fluorescence intensity changes of **1-Z** (5.0×10^{-6} M) in PBS buffer (10% DMSO, pH = 7.4), upon titration with bovine fetal albumin (0-5 equiv.).

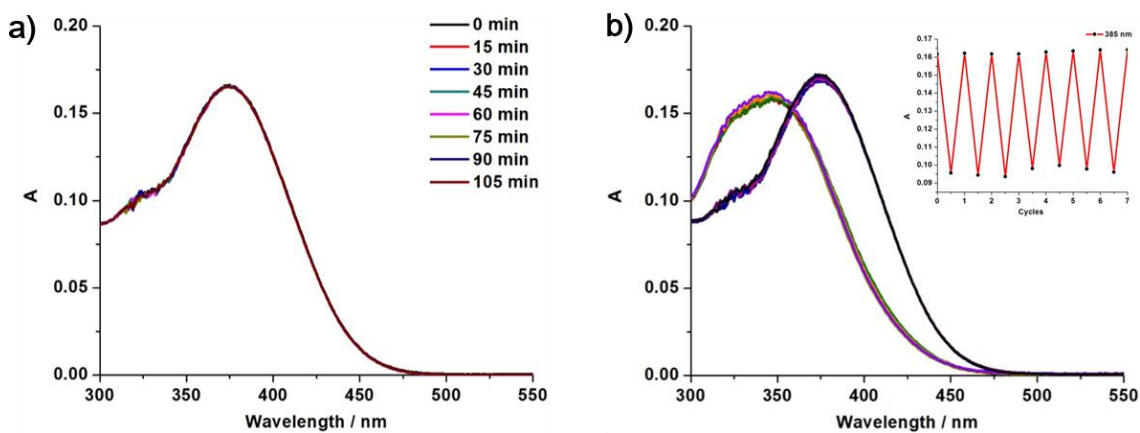


Figure S23. a) UV-Vis spectra of **1-Z** (1.0×10^{-5} M) in PBS buffer (50% MeCN, pH = 7.4) with 1000 equiv. GSH (10mM). The measurements were taken at 15-min intervals; b) UV-Vis spectra of the switching cycles of **1** (1.0×10^{-5} M) in PBS buffer (50% MeCN, pH = 7.4); The inset shows the isomerization cycles of **1** in PBS buffer (50% MeCN, pH = 7.4) upon irradiation with alternated 442 nm and 340 nm light sources. The absorbance change at $\lambda_{\max} = 385$ nm was monitored.

5 Photoisomerization Studies in the Solid State

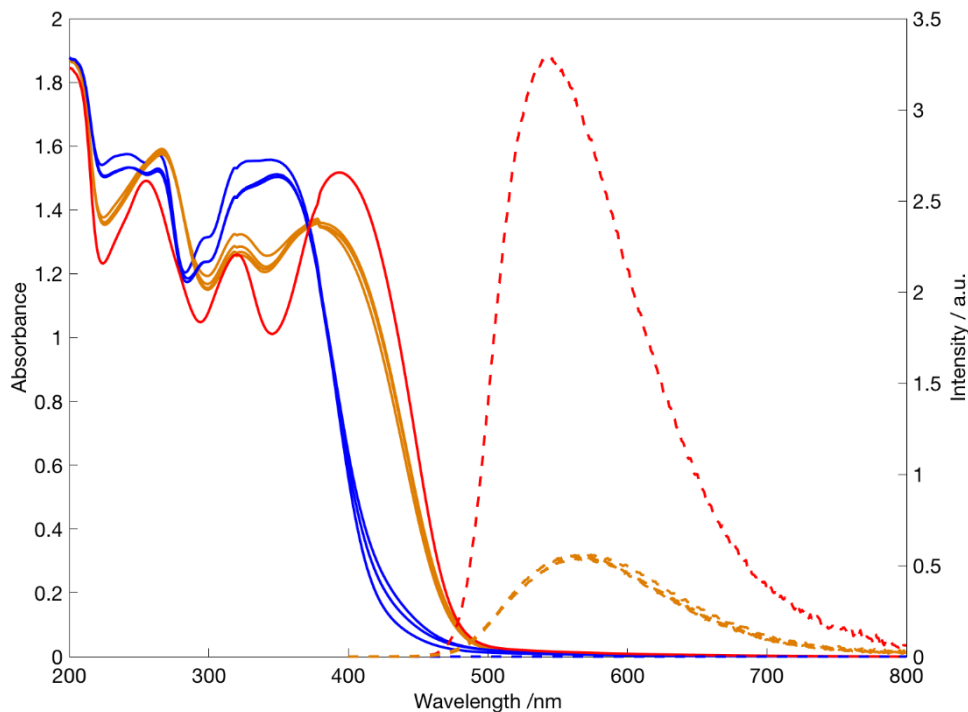


Figure S24. Absorption (left scale, solid lines) and luminescence (right scale, dashed lines; $\lambda_{\text{ex}} = 370$ nm, isosbestic point) spectral changes observed on a drop casted film of 1-Z (red lines), deposited on a glass slide, upon alternating irradiation periods at 450 nm ($Z \rightarrow E$ isomerization, blue lines) and 360 nm ($E \rightarrow Z$ isomerization, orange lines).

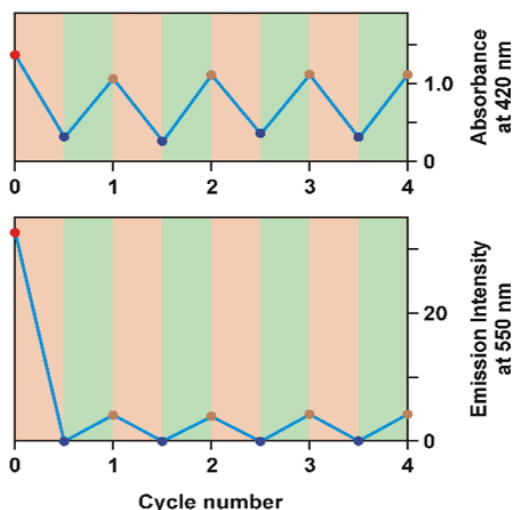
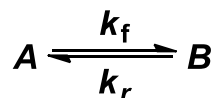


Figure S25. Absorbance (top) and emission (bottom) changes of a drop casted film of 1-Z subjected to alternative irradiation cycles at 450 and 360 nm. Orange areas: irradiation at 450 nm for 20 min. Green areas: irradiation at 360 nm for 20 min.

6 Photoisomerization Quantum Yield



In a photochemical reaction, species A absorbs light to generate the product B. The general kinetics of a basic photochemical reaction can be expressed using Eq. 1,^{S4}

$$r_{A \rightarrow B} = \frac{I_0 \Phi_{A \rightarrow B}}{V} (1 - 10^{-\varepsilon_A C_A l}) \quad \text{Eq. 1.}$$

where $r_{A \rightarrow B}$ indicates photoisomerization rate from A to B; I_0 indicates molar photon flux; $\Phi_{A \rightarrow B}$ indicates photoisomerization yield from A to B; V indicates sample volume; ε_A indicates molar absorption coefficient of sample A at irradiation wavelength; C_A indicates the concentration of sample; and l indicates the light path length. When $\varepsilon_A \cdot C_A \cdot l \cdot \ln 10 \ll 1$ (or $Abs_A \ll 0.43$), the Taylor expansion can be truncated at the first-order term, simplifying Eq. 1 to Eq. 2.

$$k_{A \rightarrow B} = \frac{I_0 \Phi_{A \rightarrow B}}{V} \varepsilon_A \cdot l \cdot \ln 10 \quad \text{Eq. 2.}$$

Rearranging Eq. 2 gives Eq. 3,

$$\Phi_{A \rightarrow B} = \frac{k_{A \rightarrow B} V}{I_0 \varepsilon_A l \ln 10} \quad \text{Eq. 3.}$$

where $\Phi_{A \rightarrow B}$ indicates the photoisomerization yield from A to B; $k_{A \rightarrow B}$ represents the rate constant (obtained from the exponential fit of a graph of Abs vs. time); V indicates sample volume; I_0 indicates molar photon flux; ε_A indicates molar absorption coefficient at irradiation wavelength; and l indicates the light path length.

The molar photon flux I_0 at 340 and 442 nm were determined using chemical actinometry.^{S5} A 0.002 L (= V_0) solution of potassium ferrioxalate in 0.05 M H_2SO_4 was placed in a 1.0 cm cuvette and irradiated for 30 s (= t_0). The irradiated solution was combined with 3.5 equiv. of ferrozine and stirred under the dark for an hour. The resulting solution, containing reddish-purple $[Fe(\text{ferrozine})_3]^{2+}$ complex, was diluted by a factor of 30 (= n), and its absorbance was measured at 563 nm (A_{563}), where its molar absorption coefficient (ε_{563}) is 27,900 $cm^{-1} M^{-1}$. The molar

photon flux I_0 of light source at different wavelengths was determined using the following Eq. 4.

$$I_0 \left(mol \cdot s^{-1} \right) = \frac{A_{563} \cdot n \cdot V_0}{\varepsilon_{563} \cdot l \cdot t_0 \cdot \phi_\lambda} \quad \text{Eq. 4.}$$

where l indicates the length of the cuvette; and ϕ_λ stands for the quantum yield of the photo-reduction of Fe(III) oxalate induced by the light source ($\phi_{340} = 1.25$ and $\phi_{442} = 1.11$). The rate law for the formation of species **B** is described in Eq. 5.

$$C_B = \frac{k_f}{k_f + k_r} C_{total} (1 - e^{-(k_f + k_r)t}) \quad \text{Eq. 5.}$$

where C_{total} is the total concentration of the photoswitch ($C_A + C_B$), and k_f and k_r are the first order approximate rate constants for the forward and reverse photochemical reactions under the low absorption approximation discussed above.

Rearranging Eq. 5 gives the rate law for the formation of species **A** (Eq. 6),

$$C_A = \frac{C_{total} \cdot k_r}{k_f + k_r} + \frac{C_{total} \cdot k_f}{k_f + k_r} e^{-(k_f + k_r)t} \quad \text{Eq. 6.}$$

C_A is proportional to the absorbance of species **A**. An exponential fit of absorbance as a function of time gives the observed rate constant $k_{obs} = k_f + k_r$. For this family of photochromic hydrazone switches, the thermal relaxation is extremely slow at room temperature (figure S45) and so $k_{A \rightarrow B} \approx k_{obs}$.

The photoisomerization quantum yield in drop-casted thin films could not be determined because relevant parameters, such as the absorption coefficient of the compound in the film and the photon flow in the irradiated volume, are not known.

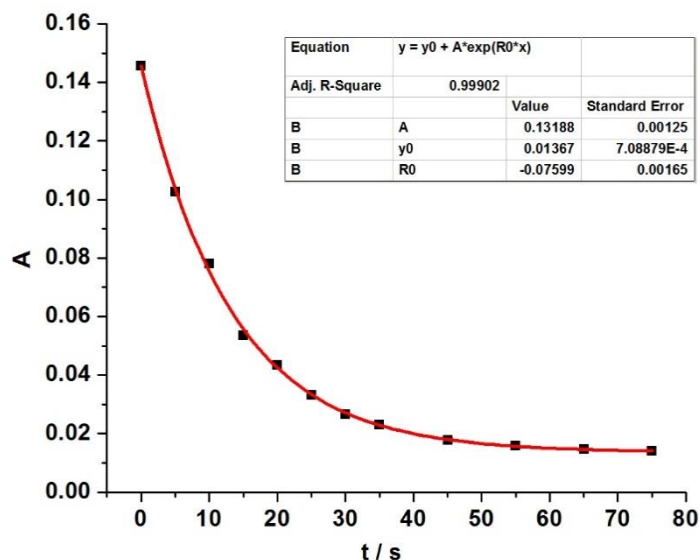


Figure S26. The photoisomerization (irradiation at 442 nm) of **1-Z** to **1-E** in toluene (1×10^{-5} M) at 298 K; the plot is of the absorbance ($\lambda_{max} = 395$ nm) of **1-Z** as a function of time. $\epsilon_{1-Z@442nm} = 4305 \text{ M}^{-1} \cdot \text{cm}^{-1}$ was used for the quantum yield calculations. The photoisomerization quantum yield was calculated to be $32.0 \pm 0.9\%$ based on three consecutive measurements.

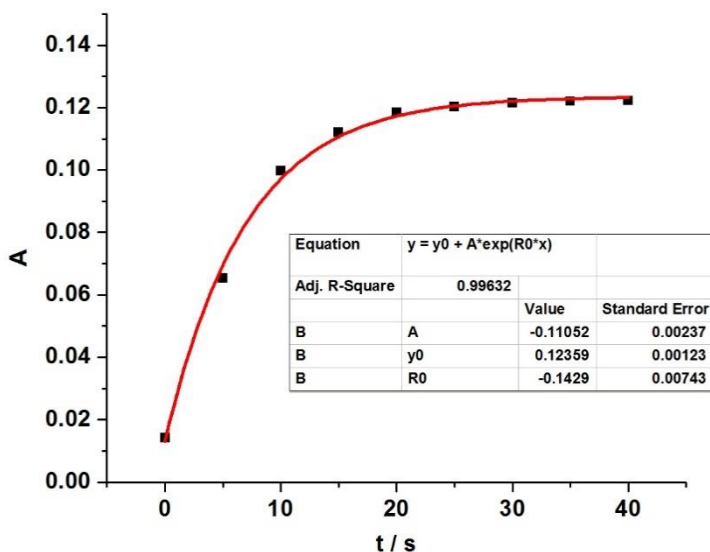


Figure S27. Kinetics for the photoisomerization (irradiation at 340 nm) of **1-E** to **1-Z** in toluene (1×10^{-5} M) at 298 K; the plot is of the absorbance ($\lambda_{max} = 395$ nm) of **1-Z** as a function of time. $\epsilon_{1-E@340nm} = 13732 \text{ M}^{-1} \cdot \text{cm}^{-1}$ was used for the quantum yield calculations. The photoisomerization quantum yield was calculated to be $14.7 \pm 1.0\%$ based on three consecutive measurements.

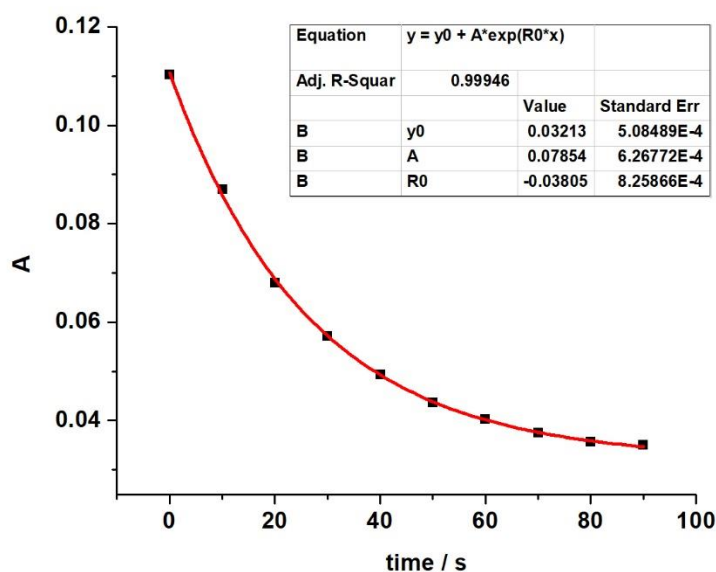


Figure S28. The photoisomerization (irradiation at 442 nm) of **1-Z** to **1-E** in 10% FBS buffer (1×10^{-5} M) at 298 K; the plot is of the absorbance ($\lambda_{max} = 395$ nm) of **1-Z** as a function of time. $\epsilon_{1-Z \text{ in serum@442nm}} = 3905 \text{ M}^{-1} \cdot \text{cm}^{-1}$ was used for the quantum yield calculations. The photoisomerization quantum yield was calculated to be $18.9 \pm 0.8\%$ based on three consecutive measurements.

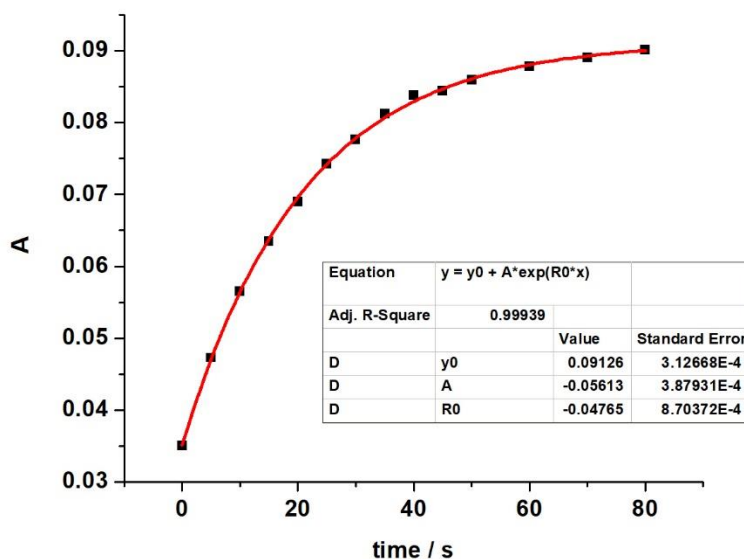


Figure S29. Kinetics for the photoisomerization (irradiation at 340 nm) of **1-E** to **1-Z** in 10% FBS buffer (1×10^{-5} M) at 298 K; the plot is of the absorbance ($\lambda_{max} = 395$ nm) of **1-Z** as a function of time. $\epsilon_{1-E \text{ in serum@340nm}} = 11194 \text{ M}^{-1} \cdot \text{cm}^{-1}$ was used for the quantum yield calculations. The photoisomerization quantum yield was calculated to be $6.9 \pm 0.3\%$ based on three consecutive

measurements.

7 Fluorescence Emission Properties

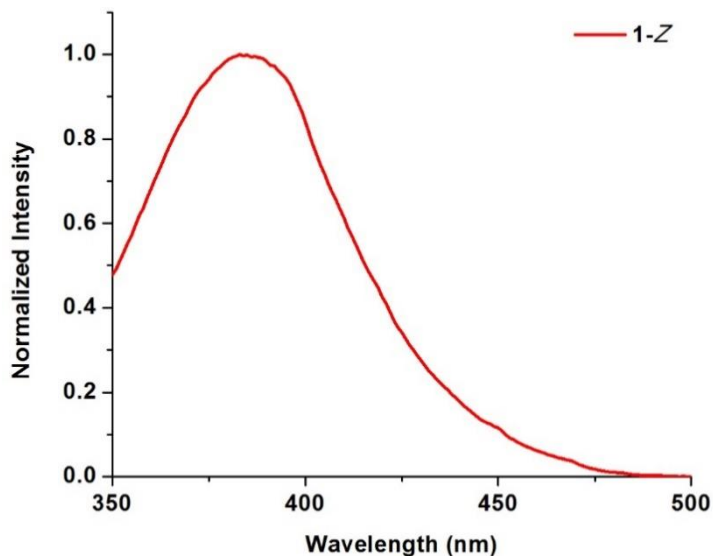


Figure S30. Excitation spectrum of **1-Z** (5×10^{-6} M) in toluene with $\lambda_{em} = 525$ nm.

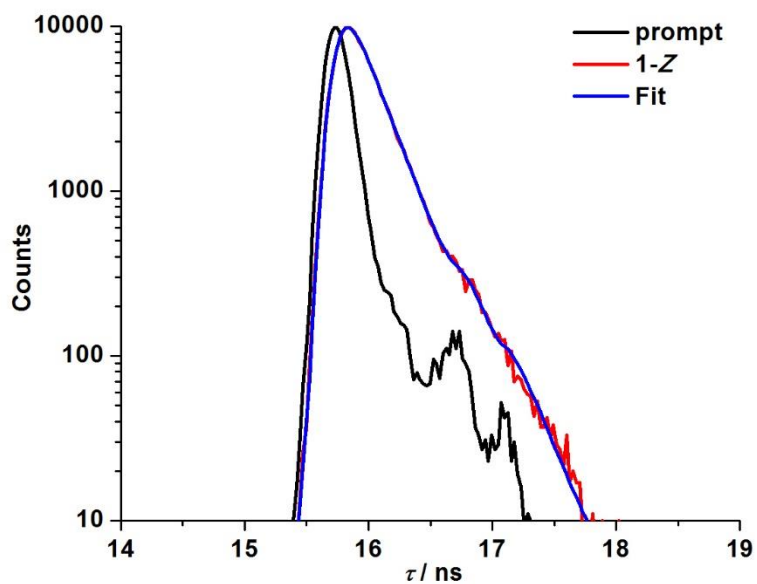


Figure S31. Fluorescence lifetime decay of **1-Z** (5×10^{-6} M) in toluene. The fluorescence decay lifetime was determined to be 193 ± 2 ps based on three consecutive measurements.

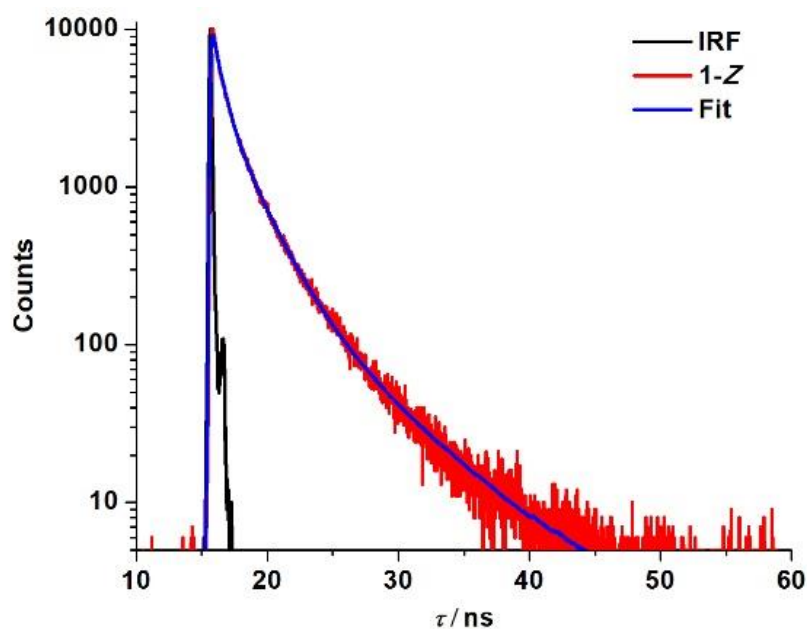


Figure S32. Fluorescence lifetime decay of **1-Z** (5×10^{-6} M) in 10% FBS buffer. Multi-exponential fitting ($\chi^2 = 1.9$) gave fluorescence decay lifetimes of 5.97 ± 0.11 ns ($3.2 \pm 0.2\%$), 0.59 ± 0.01 ns ($64.7 \pm 0.5\%$) and 2.11 ± 0.03 ns ($32.1 \pm 0.5\%$) - the pre-exponential factors are shown in brackets.

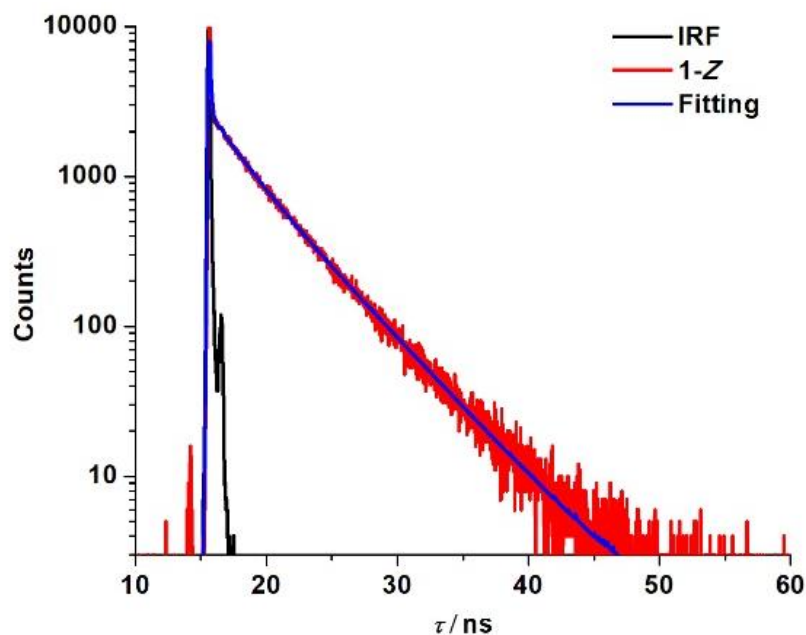


Figure S33. Fluorescence lifetime decay of powder (**1-Z**). Multi-exponential fitting ($\chi^2 = 1.1$) gave fluorescence decay lifetimes of 2.28 ± 0.11 ns ($3.5 \pm 0.2\%$), 0.07 ± 0.01 ns ($90.2 \pm 3.1\%$) and 4.73 ± 0.05 ns ($6.3 \pm 0.2\%$) - the pre-exponential factors are shown in brackets.

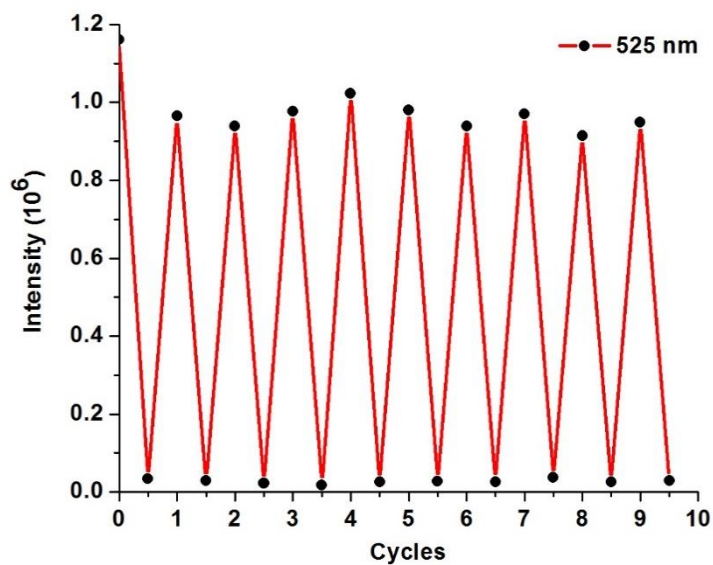


Figure S34. The ON/OFF fluorescence switching cycles of switch **1** in toluene. The fluorescence intensity change at $\lambda = 525$ nm was monitored using a fluorimeter while alternating the irradiation wavelength between 442 and 340 nm.

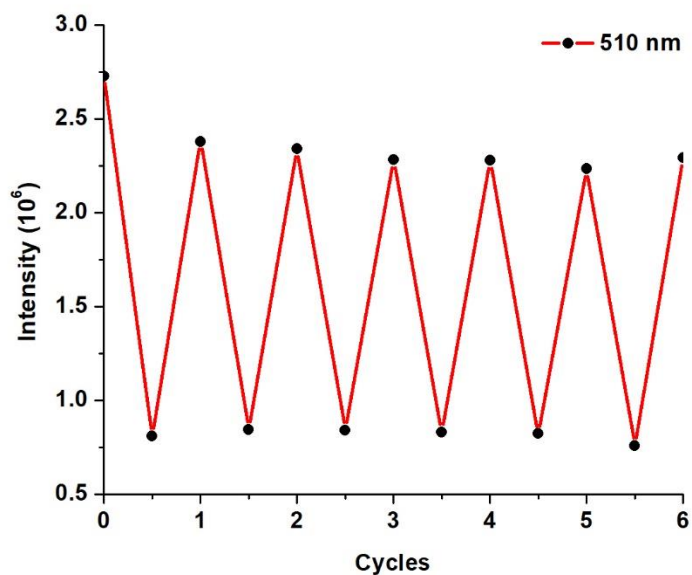


Figure S35. The ON/OFF fluorescence switching cycles of switch **1** in 10% FBS buffer. The fluorescence intensity change at $\lambda = 510$ nm was monitored using a fluorimeter while alternating the irradiation wavelength between 442 and 340 nm.

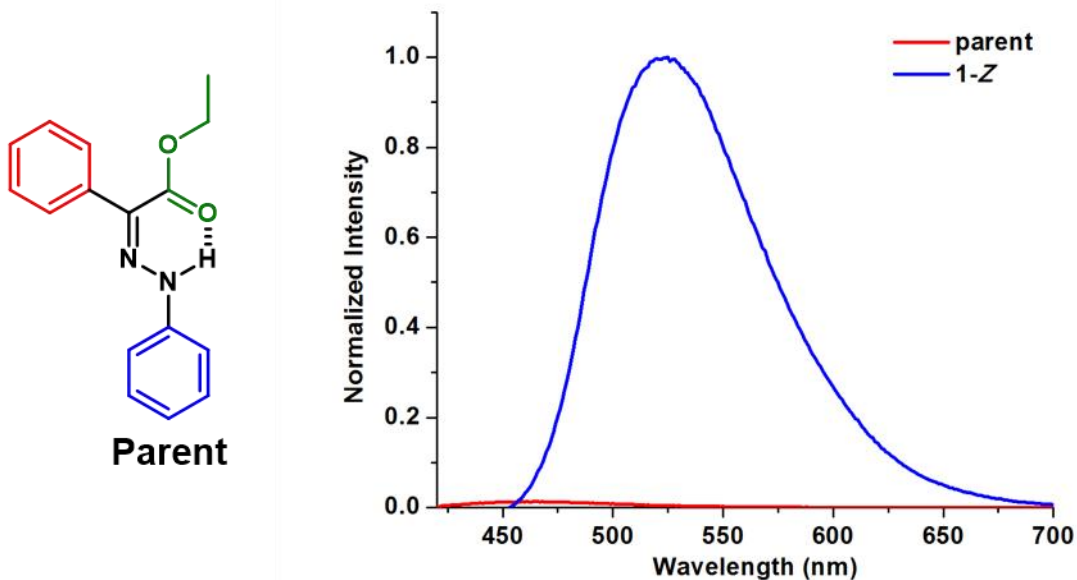


Figure S36. Fluorescence spectrum of **parent** hydrazone (red; 5×10^{-6} M) and **1-Z** (blue; 5×10^{-6} M) in toluene at $\lambda_{\text{ex}} = 367$ nm, and $\lambda_{\text{ex}} = 420$ nm, respectively.

Switching of control compound **2**

To gain an insight into the emission mechanism, we synthesized the methylated compound **2** (Scheme S2). The *Z* and *E* isomers of **2** were separated and characterized using NMR spectroscopy (figs. S4 to S11) and mass spectrometry. The photoisomerization of **2** is inefficient (figure S16) because of the overlap of the UV bands of the isomers (figure S37). Moreover, no emission was observed upon excitation at the absorption maximum of either **2-Z** or **2-E** (figure S37). These results lead us to conclude that the intramolecular H-bond in **1-Z** is crucial for its fluorescence emission, giving support to the ESIPT mechanism.

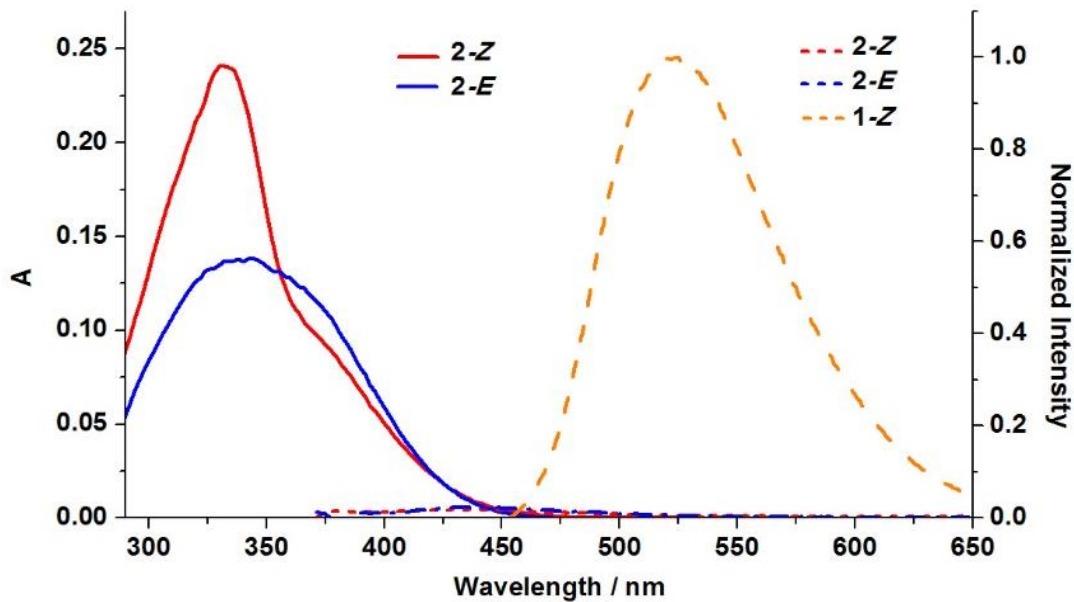


Figure S37. Normalized UV-Vis absorption spectra (solid lines; 1×10^{-5} M) and fluorescence spectra (dashed lines; 5.0×10^{-6} M) of **2-Z**, **2-E** and **1-Z** in toluene.

Solvent-dependent UV/Vis and emission spectra of **1**

The absorption and emission spectra of **1-Z** were measured in solvents having varying polarities. As shown in Figure S38, the absorption maxima of **1-Z** are slightly affected by the nature of the solvent, which indicates that its ground state has some charge transfer character. This effect is most likely stemming from the presence of the electron donating NMe₂ substituent. The largest shift in the series is observed in MeCN, which has hypsochromic shift of 17 nm as compared to toluene. The emission profile of **1-Z** on the other hand is highly dependent on solvent polarity and presence of acidic protons (Figure S39 and Table S1). As expected from the ESIPT mechanism, polar solvents lower the emission intensity and lead to bathochromic shifts with respect to non-polar solvents. Polar protic solvents, on the other hand, lead to substantial emission quenching. Compared to MeCN, solutions of **1-Z** exhibit hypsochromic shifts and intensified emission bands in apolar solvents (e.g., toluene, DCM). The biggest bathochromic shift (51 nm) in emission wavelength is found between toluene and DMSO, which indicates that a highly polarized and

distorted charge-transfer state may be formed upon excitation.^{S6} A diminished emission band was observed in H-bond acceptor solvents, e.g., dioxane and DMSO. More importantly, it was found that the fluorescence emission of **1-Z** was quenched to a large extent in polar protic solvents (e.g. methanol and ethanol). These results yet again lend credence to our hypothesis that ESIPT coupled with charge transfer from NMe₂ might be responsible for the observed emission in **1-Z**.

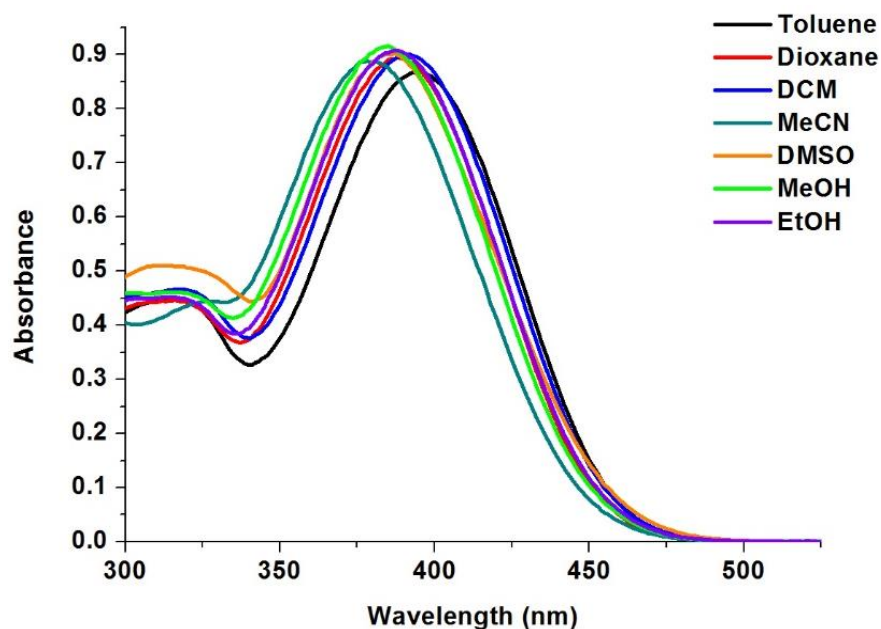


Figure S38. Solvent-dependent UV-Vis absorption spectra of **1-Z** (5×10^{-5} M) in different solvents.

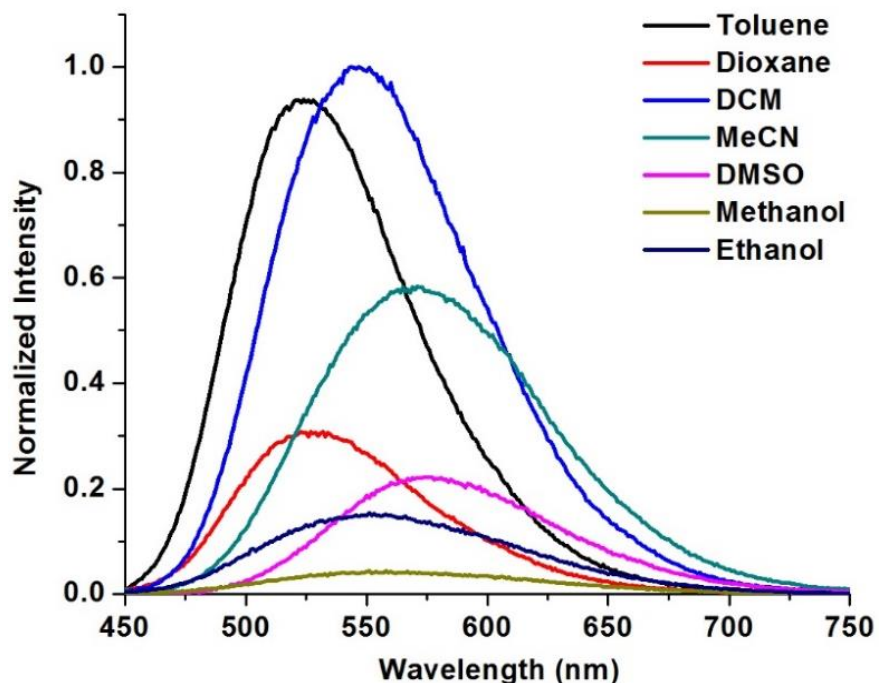


Figure S39. Solvent-dependent fluorescence emission of **1-Z** (1.0×10^{-5} M). Absorption maxima (λ_{max}) of **1-Z** in corresponding solvents (figure S38) were used as the excitation wavelengths.

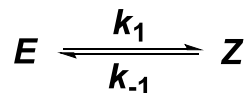
Table S1. Emission maxima of **1-Z** (1×10^{-5} M) and their corresponding intensities in various solvents. The absorption maxima of **1-Z** in the different solvents were used as the excitation wavelengths.

	Toluene	Dioxane	DCM	MeCN	DMSO	MeOH	EtOH
λ_{ex}/nm	395	388	392	378	387	385	388
λ_{em}/nm	524	527	544	571	575	551	558
Relative Intensity ^a	0.95	0.31	1	0.62	0.22	0.04	0.16

^a The fluorescence intensity of **1-Z** in DCM was set to 1.

8 Kinetic Studies

The thermal isomerization rate of **1** was studied using variable temperature ^1H NMR spectroscopy. Solutions of switch **1** (1×10^{-3} M) in toluene- d_8 were irradiated with 442 nm light, and then left in a Haake F3 circulating oil bath at a preset temperature. ^1H NMR spectra were then acquired at different intervals at room temperature to monitor the change in ester CH_2 proton signal intensity as a function of time. The time that each measurement takes (~ 5 min) is much shorter than the half-life of the hydrazone switch at room temperature, and so was ignored when processing the data. Changes in the intensity of the ester CH_2 protons were used to calculate the ratio and concentration of the *Z* and *E* isomers. The thermal isomerization rates (k) were determined by least-square curve fittings using an integrated and combined rate equation of a single-species reversible reaction (Eq. 9).^{S7}



$$K_{eq} = \frac{k_1}{k_{-1}} = \frac{C_A^0 - C_A^{eq}}{C_A^{eq}} \quad \text{Eq. 7}$$

$$\ln\left(\frac{C_A - C_A^{eq}}{C_A^0 - C_A^{eq}}\right) = -(k_1 + k_{-1})t \quad \text{Eq. 8}$$

Combining Eq. 7 and 8 will give Eq. 9.

$$C_A = (C_A^0 - C_A^{eq}) \times e^{\left(\frac{-k_1 \cdot C_A^0 \cdot t}{C_A^0 - C_A^{eq}}\right)} + C_A^{eq} \quad \text{Eq. 9}$$

where C_A , C_A^0 , and C_A^{eq} stand for experimental, initial, and equilibrium concentrations of the metastable configuration of the hydrazone switch, respectively; t stands for the thermal relaxation time.

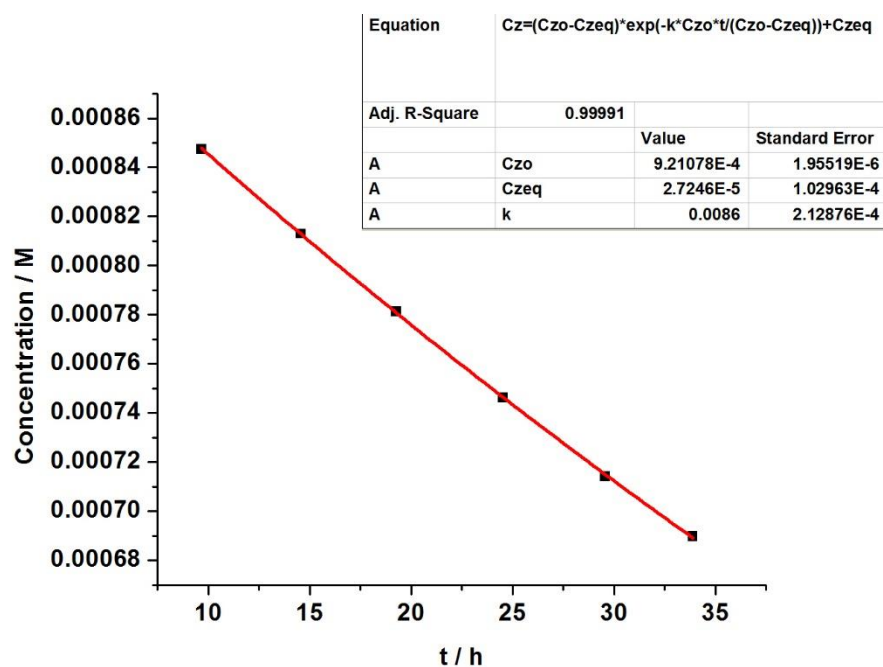


Figure S40. Thermal isomerization of **1-E** \rightarrow **1-Z** in toluene- d_8 at 368 K. The plot is of the concentration of **1-E** as a function of time.

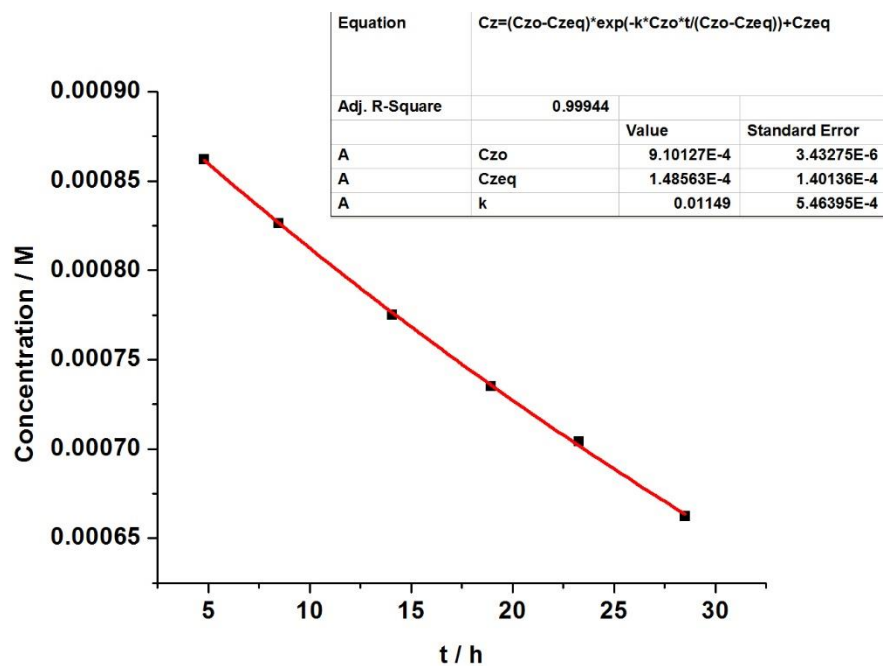


Figure S41. Thermal isomerization of **1-E** \rightarrow **1-Z** in toluene- d_8 at 371 K. The plot is of the concentration of **1-E** as a function of time.

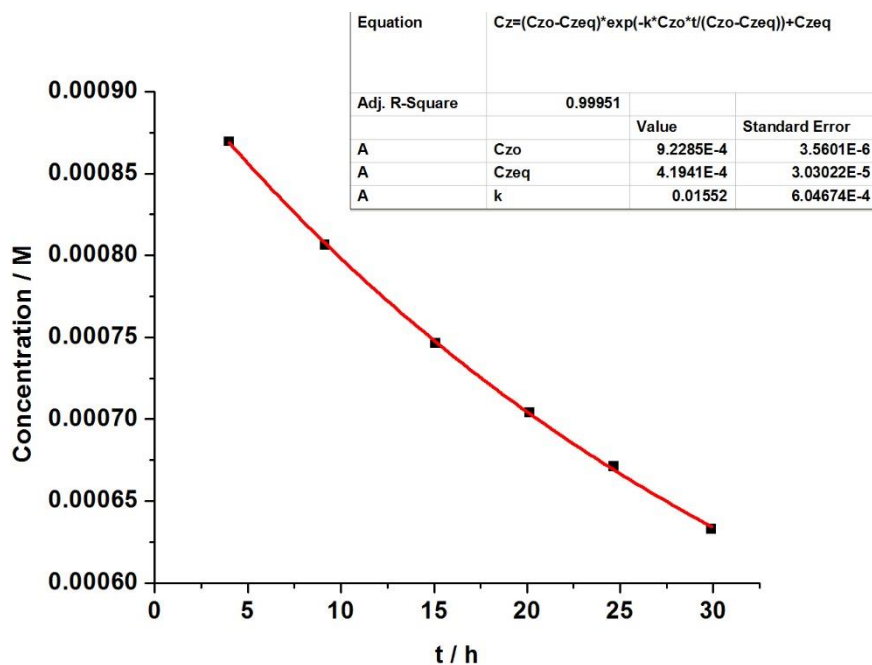


Figure S42. Thermal isomerization of **1-E** \rightarrow **1-Z** in toluene- d_8 at 374 K. The plot is of the concentration of **1-E** as a function of time.

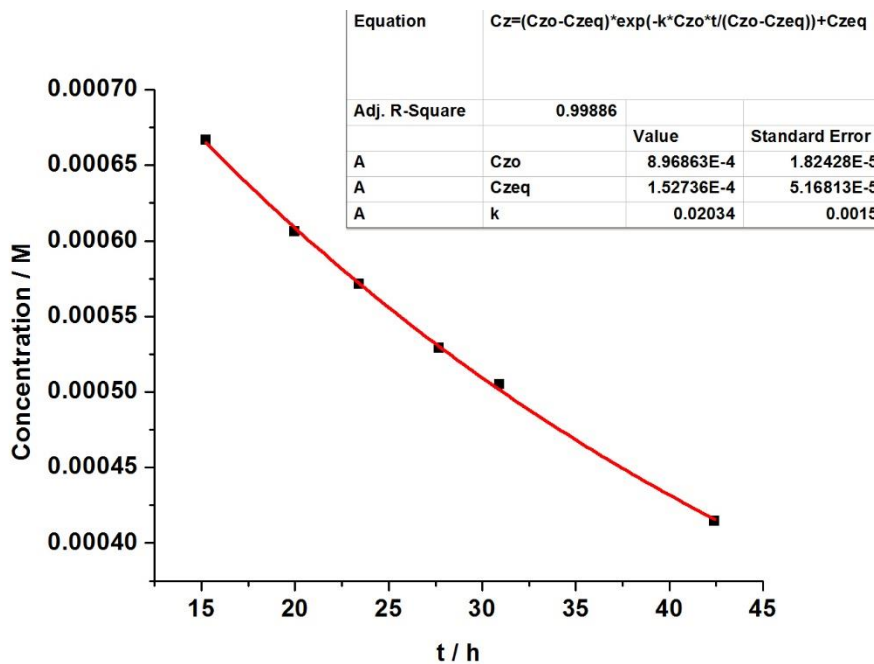


Figure S43. Thermal isomerization of **1-E** \rightarrow **1-Z** in toluene- d_8 at 377 K. The plot is of the concentration of **1-E** as a function of time.

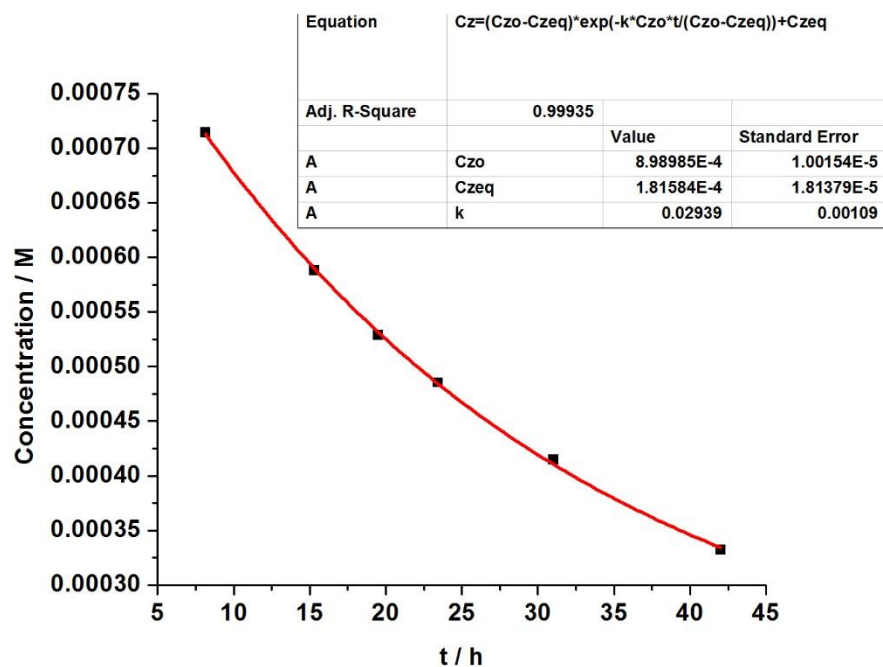


Figure S44. Thermal isomerization of **1-E** \rightarrow **1-Z** in toluene- d_8 at 380 K. The plot is of the concentration of **1-E** as a function of time.

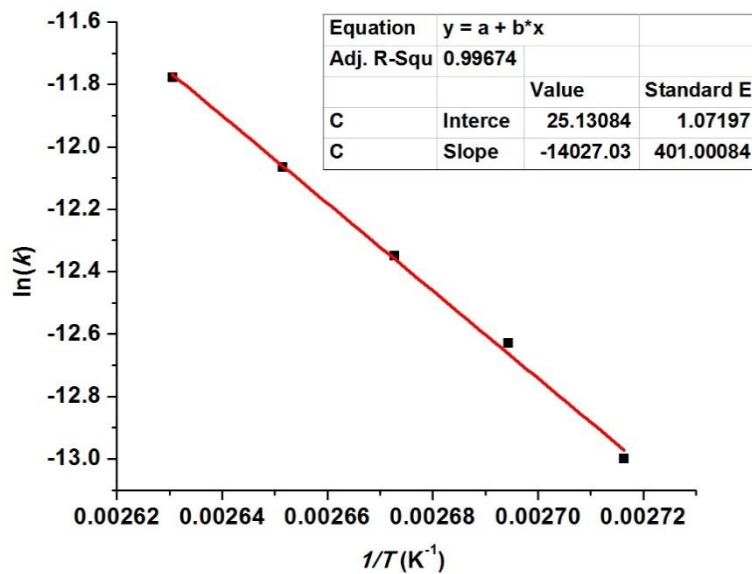


Figure S45. Arrhenius plot of the thermal isomerization of **1-E** \rightarrow **1-Z** in toluene- d_8 .

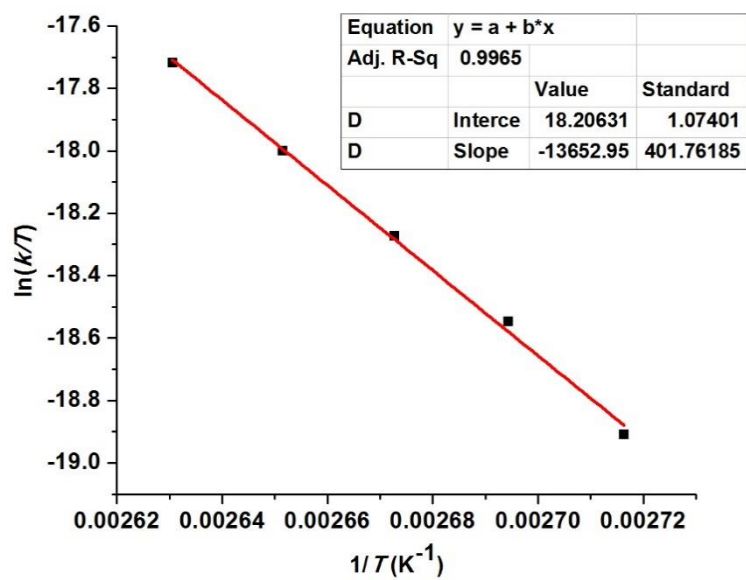


Figure S46. Eyring plot of the thermal isomerization of **1-E** \rightarrow **1-Z** in toluene- d_8 .

9 Crystallography

9.1 Crystallography information for 1-Z

A yellow needle-shaped crystal with dimensions (0.26×0.03×0.02) mm³ was mounted on a nylon loop with paratone oil. Data were collected using a Bruker APEX-II CCD diffractometer equipped with an Oxford Cryosystems low-temperature apparatus operating at $T = 173(2)$ K. Data were measured using scans of 1.00° per frame for 45.00 s using CuK α radiation (sealed tube, 40 kV, 30 mA). The total number of runs and images was based on the strategy calculation from the program **COSMO** (BRUKER, V1.61, 2009).^{S8} The actually achieved resolution was $\Theta = 70.291$. Cell parameters were retrieved using the **SAINT** (Bruker, V8.34A, 2013) software and refined using **SAINT** (Bruker, V8.34A, 2013) on 1415 reflections, 15% of the observed reflections.^{S9} Data reduction was performed using the **SAINT** (Bruker, V8.34A, 2013) software which corrects for Lorentz polarisation. The final completeness is 97.20 out to 70.291 in Θ . The absorption coefficient (μ) of this material is 0.669 at this wavelength ($\lambda = 1.54178$ Å) and the minimum and maximum transmissions are 0.6658 and 0.7533. The structure was solved in the space group P-1 (# 2) by Direct Methods using the **ShelXS** (Sheldrick, 2008) structure solution program^{S10} and refined by Least Squares using version 2014/6 of **XL** (Sheldrick, 2008) incorporated in **Olex2**.^{S11} All non-hydrogen atoms were refined anisotropically. Hydrogen atom positions were calculated geometrically and refined using the riding model.

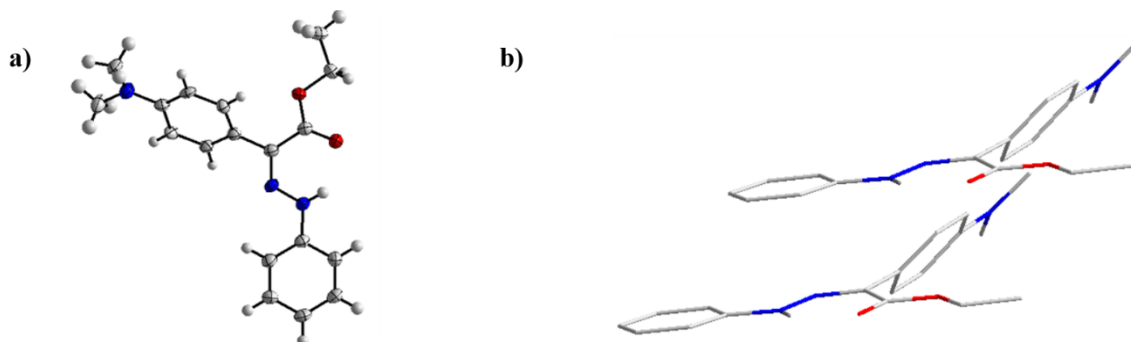


Figure S47. a) ORTEP drawing (50% probability) of the crystal structure of 1-Z; b) Crystal packing of hydrazone 1-Z (all the C-H protons have been removed for clarification).

Table S2. Crystal data and structure refinement for 1-Z

CCDC	1580327
Empirical formula	C ₁₈ H ₂₁ N ₃ O ₂
Formula weight	311.38
Temperature	173(2) K
Crystal system	Triclinic
Space group	P-1
Unit cell dimensions	4.9956(2) Å 9.5201(4) Å 17.7596(7) Å 102.122(3)° 92.757(3) ° 90.570(3)°
Volume	824.66(6) Å ³
Z	2
Z'	1
Density (Calcd.)	1.254 g/cm ⁻³
Absorption coefficient	0.669 mm ⁻¹
Crystal size	0.26×0.03×0.02 mm ³
θ range for data collection	2.548 to 70.291°
Index ranges	-6 ≤ h ≤ 6 -11 ≤ k ≤ 11 0 ≤ l ≤ 21
Reflections Measured	9656
Independent reflections	3011 [R _{int} = 0.0822, R _{sigma} = 0.0773]
Data / restraints / parameters	1690 / 0 / 271
Goodness-of-fit on F ²	0.977
Final R indexes [I ≥ 2σ (I)]	R ₁ = 0.0585, ωR ₂ = 0.1267
Final R indexes [all data]	R ₁ = 0.1159, ωR ₂ = 0.1527
Largest diff. peak and hole	0.171 and -0.199 e Å ⁻³

9.2 Crystallography information for 2-Z

A yellow chunk-shaped crystal with dimensions (0.43×0.40×0.39) mm³ was mounted on a nylon loop with paratone oil. Data were collected using a Bruker APEX-II CCD diffractometer equipped with an Oxford Cryosystems low-temperature apparatus operating at $T = 173(2)$ K. Data were measured using scans of 1.00° per frame for 110.00 s using CuK α radiation (sealed tube, 40 kV, 30 mA). The total number of runs and images was based on the strategy calculation from the program **COSMO** (BRUKER, V1.61, 2009).^{S8} The actually achieved resolution was $\theta = 72.191$. Cell parameters were retrieved using the **SAINT** (Bruker, V8.34A, 2013) software and refined using **SAINT** (Bruker, V8.34A, 2013) on 9904 reflections, 55% of the observed reflections.^{S9} Data reduction was performed using the **SAINT** (Bruker, V8.34A, 2013) software which corrects for Lorentz polarisation. The final completeness is 99.80 out to 72.191 in θ . The absorption coefficient (μ) of this material is 0.646 at this wavelength ($\lambda = 1.54178$ Å) and the minimum and maximum transmissions are 0.6766 and 0.7536. The structure was solved in the space group $P2_1/C$ (# 14) by Direct Methods using the **ShelXS** (Sheldrick, 2008) structure solution program^{S10} and refined by Least Squares using version 2014/6 of **XL** (Sheldrick, 2008) incorporated in **Olex2**.^{S11} All non-hydrogen atoms were refined anisotropically. Hydrogen atom positions were calculated geometrically and refined using the riding model.

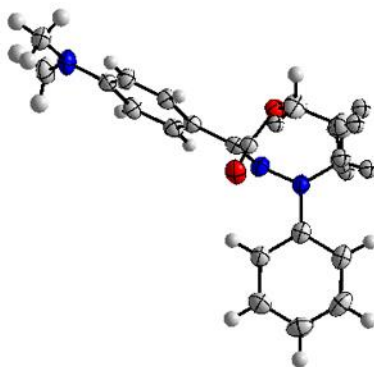


Figure S48. ORTEP (50% probability) drawing of the crystal structure of 2-Z.

Table S3. Crystal data and structure refinement for 2-Z

CCDC	1580328
Empirical formula	C ₁₉ H ₂₃ N ₃ O ₂
Formula weight	325.40
Temperature	173(2) K
Crystal system	Monoclinic
Space group	<i>P</i> 2 ₁ / <i>C</i>
Unit cell dimensions	13.9142(2) Å 8.66870(10) Å 15.2614(2) Å 90° 106.4280(10) ° 90°
Volume	1765.65(4) Å ³
<i>Z</i>	4
<i>Z</i> '	1
Density (Calcd.)	1.224 g/cm ⁻³
Absorption coefficient	0.646 mm ⁻¹
Crystal size	0.43×0.40×0.39 mm ³
θ range for data collection	3.311 to 72.191°
Index ranges	-16 ≤ <i>h</i> ≤ 17 -10 ≤ <i>k</i> ≤ 10 -18 ≤ <i>l</i> ≤ 18
Reflections Measured	17872
Independent reflections	3458 [<i>R</i> _{int} = 0.0296, <i>R</i> _{sigma} = 0.0239]
Data / restraints / parameters	3019/ 0 / 221
Goodness-of-fit on <i>F</i> ²	1.039
Final <i>R</i> indexes [<i>I</i> ≥ 2σ(<i>I</i>)]	<i>R</i> ₁ = 0.0361, ω <i>R</i> ₂ = 0.0940
Final <i>R</i> indexes [all data]	<i>R</i> ₁ = 0.0416, ω <i>R</i> ₂ = 0.0982
Largest diff. peak and hole	0.168 and -0.165 e Å ⁻³

10 Writing in Solution

To demonstrate the combined benefit of bistability and ON/OFF fluorescence switching in **1**, we used it in a reversible solution-based writing-and-recording system. A laser pointer ($\lambda = 450$ nm) was utilized as a “pen”, a 365nm UV lamp was used as a reading/erasing platform, and toluene was used as canvas. A toluene solution of **1** was irradiated under the UV light leading to fluorescence emission. The laser pointer was then used to draw different patterns in the solution by quenching the emission using the “pen” strokes (Figure S49 and VideoS1). When the UV light is turned off at this stage the drawing persists in solution for up to an hour, after which diffusion erases it (Figure S51 and Video S2). It is noteworthy that the **1-E** molecules formed through this process persist in solution because of their long-thermal lifetime, and the apparent quenching mainly results from diffusion assisted dilution of **1-E**. Another way to erase the drawings is to keep the UV light on, which will lead to $E \rightarrow Z$ isomerization and turn ON the emission at the quenched areas. This technique was used to exploit the toluene canvas in multiple write-erase cycles (Figure S50).

Experimental setup: Spectrophotometric grade toluene was used for the solution writing experiments. A solution of **1** (40 mL, 1.0×10^{-4} M) in toluene was prepared and transferred into a rectangular glass container and used as a writing substrate (canvas). The solution thickness was set at around 0.5 cm. The glass container was then placed under 365 nm UV lamp, and a 450 nm laser pointer was applied to do the writing (figure S49, video S1).

When the UV lamp is turned off after writing and the whole setup left under dark, then the writing will disappear in ca. 1 hour as a result of diffusion (figure S51, video S2). When left under the UV light, the writing will disappear after ca. 15 mins, because of the $E \rightarrow Z$ isomerization.



Figure S49. The set-up of writing in solution. The glass container was placed beneath the 365 nm UV lamp, which was set up to excite **1** so it will emit fluorescence, and subsequently isomerize thus erasing the writing.

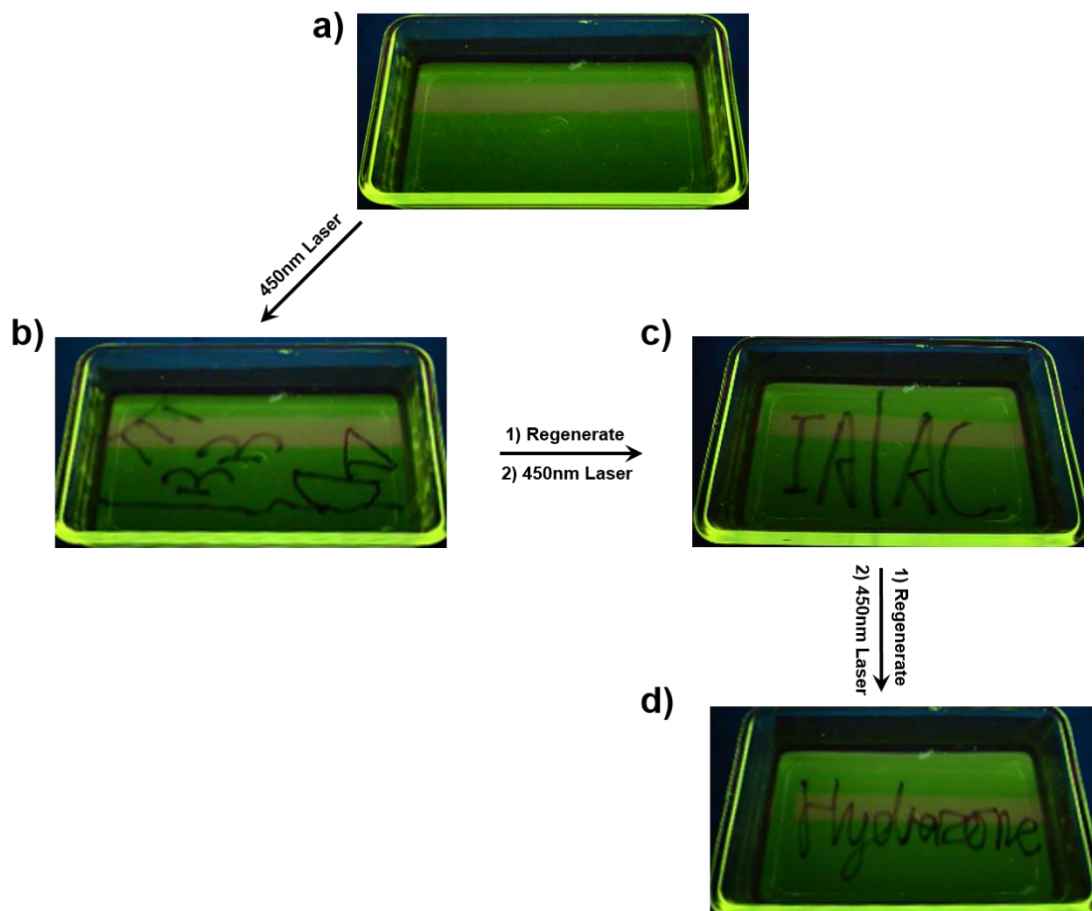


Figure S50. Writing in solution experiment. a) Solution before writing; b-d) three different words/patterns were drawn one after another, using the same toluene solution of **1**. The UV lamp was on throughout the write/erase cycles.

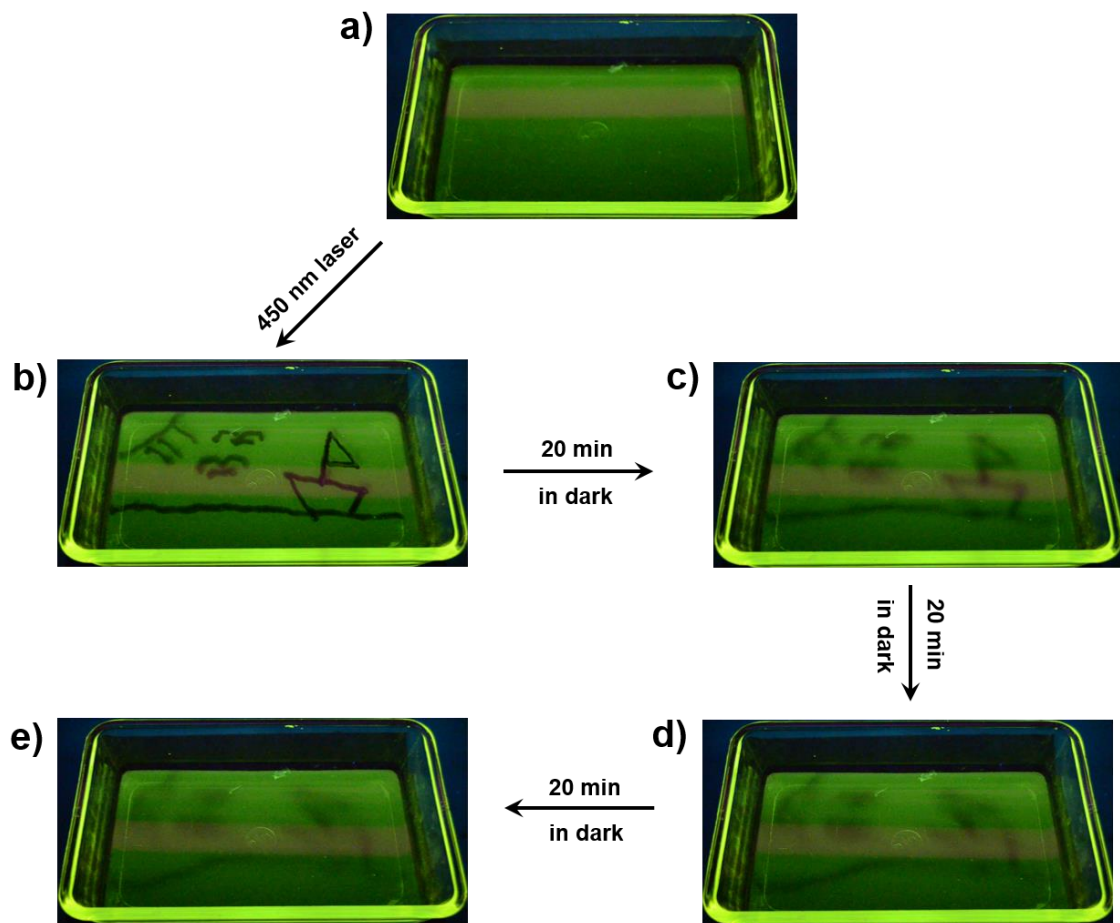


Figure S51. Writing in solution control experiment. a) Before writing; b) after writing; at c) 20-min d) 40-min and e) 60-min interval after writing. The UV light was turned OFF during intervals and only turned ON every 20 minutes to capture the changes in image.

11 Solid-State Imaging

To take advantage of the solid-state switching of **1** and accompanied ON/OFF emission toggling, we used it as a solid dye on different surfaces. In the first case we soaked a filter paper with a dichloromethane solution of **1** and let it dry under air. Once completely dry, we covered the paper with a mask and irradiated it with 442 nm light to quench the fluorescence of the unmasked area. Removing the mask and observing the filter paper under 365 nm UV lamp, showed an emissive pattern that matches the mask (Figure S53). Continued exposure under a 365 nm UV lamp erases the writing allowing for the cycling of this process with other masks. In another instance we coated **1** on a transparency film and used a laser pointer to draw pictures by quenching the emission at the “pen” strokes (Figure S55 and Video S3). Again, UV light was used to visualize, and depending on exposure time eventually erase the drawing. These two simple demonstrations show how easily the solid-state properties of **1** can be taken advantage of.

Experimental setup for filter paper writing: Glass microfiber filters (circle, diameter = 42.5mm) from Whatman[®] were used for the preparation of the hydrazone-deposited filters. A solution of **1-Z** (5.0×10^{-4} M) in dichloromethane (spectroscopic grade) was prepared, and the filters were fully immersed into the solution for approx. 10s, and then left to air-dry. The resulting hydrazone-deposited filters were used for the solid-state photomask imaging experiments.

The mask was placed on the filter paper (figure S52), and then the laser pointer was applied to thoroughly erase the unmasked area. The mask was then removed and the filter paper was placed under the 365 nm UV lamp to visualize the fluorescent image. Exposure under 365 nm UV lamp for several minutes leads to the recovery of background fluorescence. A second mask having a different pattern was then placed onto the same filter paper for another write/erase cycle. This process was repeated at least 7 times using the same filter paper (figure S53).



Figure S52. The set-up of photomask studies. The filter paper was placed on a slanted platform, and the 365 nm UV lamp was anchored above the photomask platform for the readout and fluorescence recovery cycles. The laser pointer was used to erase the emission around the mask.

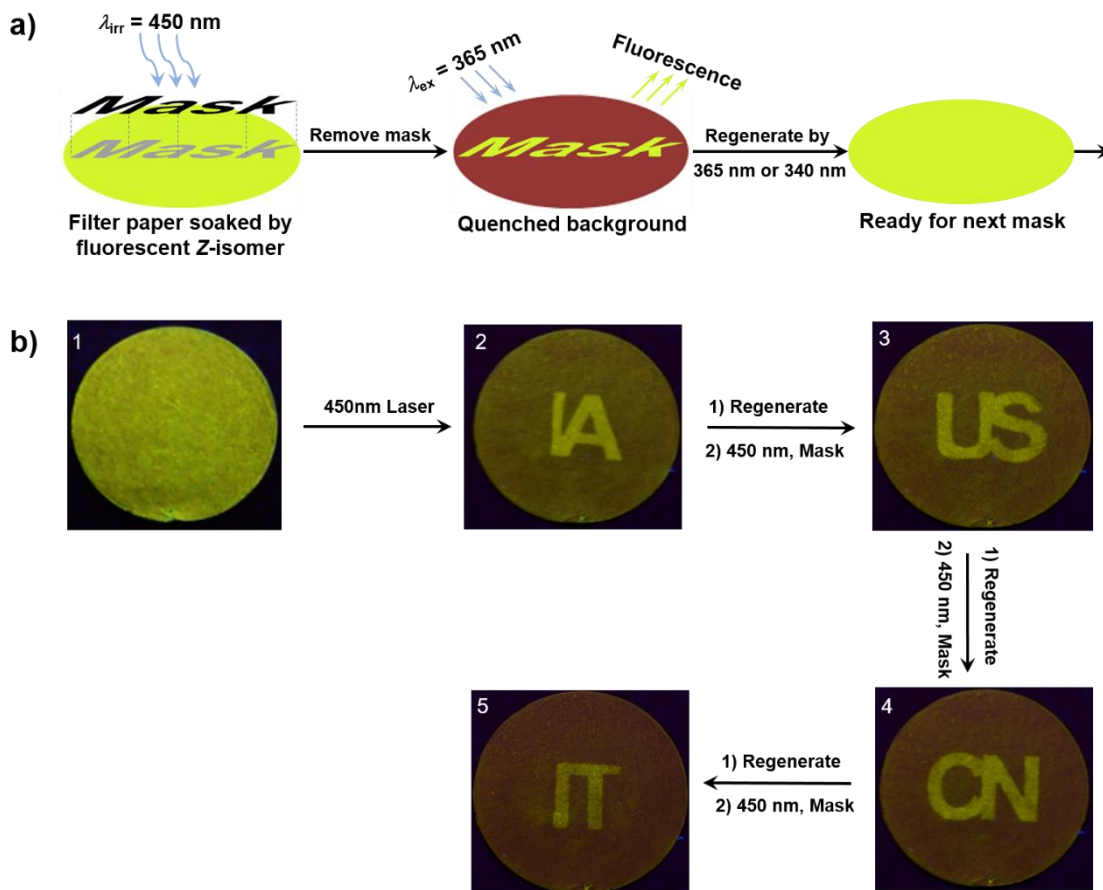


Figure S53. Photomasks on a single filter paper. a) The mask was put on the filter paper and surrounding area was irradiated with 450 nm. Removing the mask and monitoring under 365 nm showed the image left behind, which disappeared with time. b) Original filter paper (1) and four photomasks (2-5) were used for the write/erase cycles using the same filter paper.

Experimental setup for transparency film writing: A solution of **1** (3.0×10^{-3} M) in dichloromethane was prepared, and 5-10 mL of it were dispersed on a transparency slide. After the DCM evaporated, a thin layer of **1-Z** was deposited onto the transparency slide.

The transparency slide was then anchored on a 365 nm UV lamp (figure S54). A laser pointer was used to write on the slide (video S3). The images were made visible by the excitation of UV light. Long exposure to the light erases the writing, allowing for another write/erase cycle (figure S55 and Video S3).

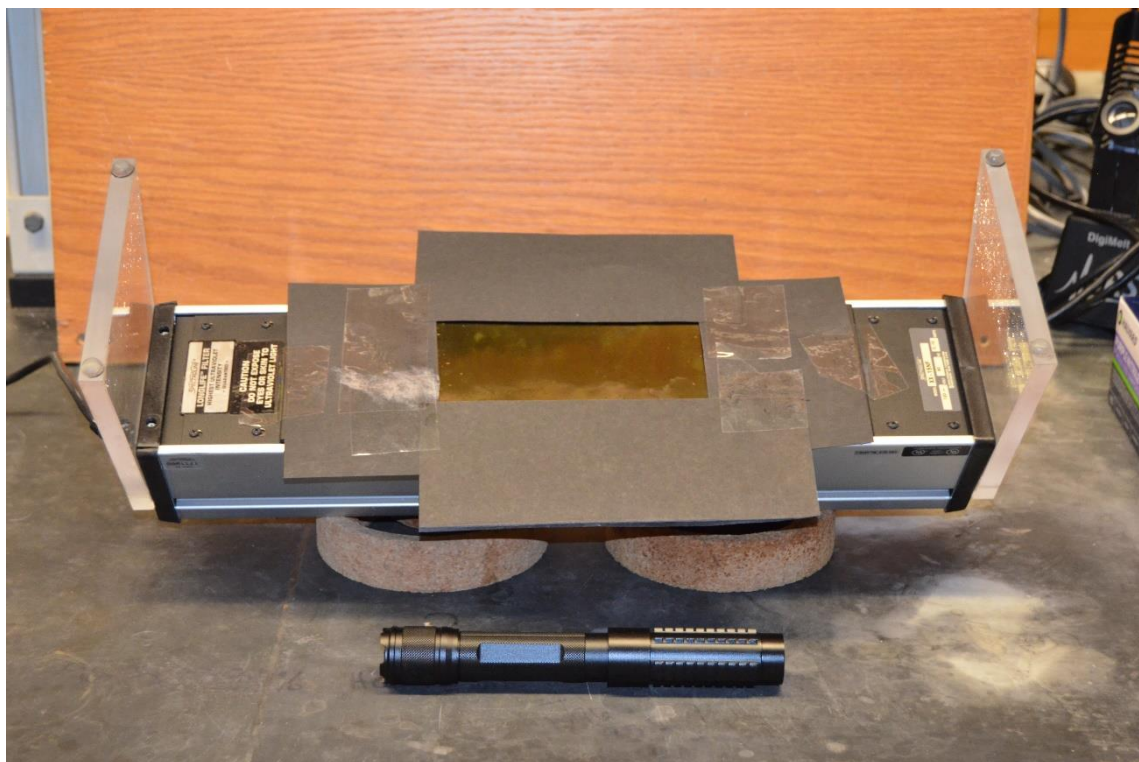


Figure S54. The set-up of writing in solid state. The transparency slide covered with **1-Z** was placed on a 365nm UV lamp, which was used to both excite the molecules to enable reading, and to erase the writing.

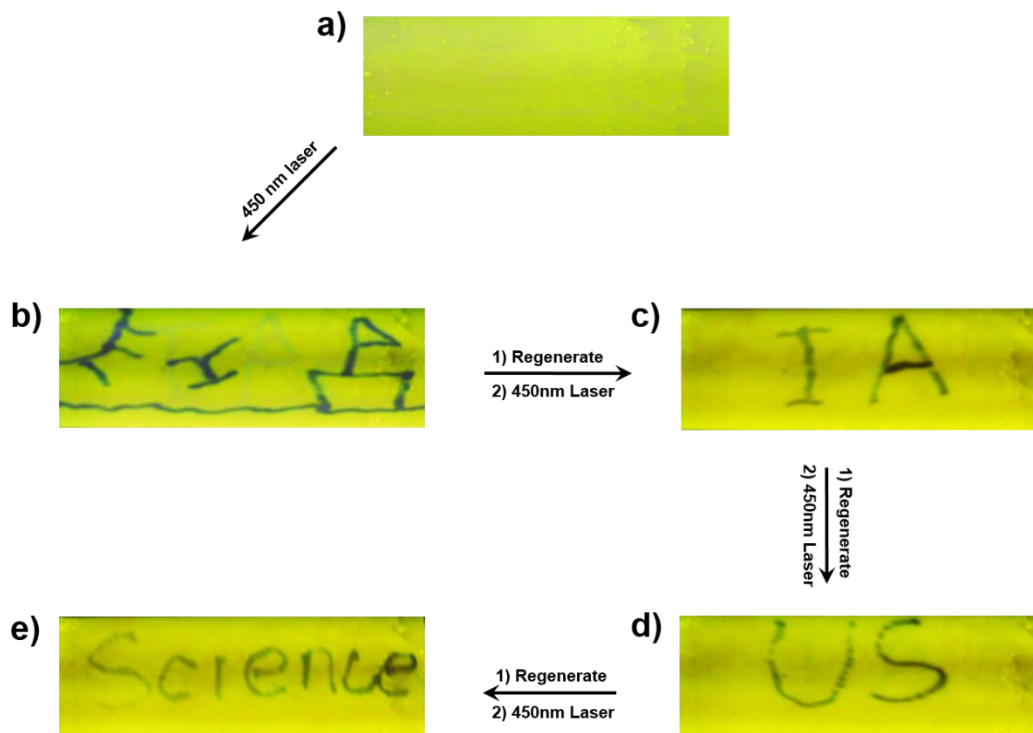


Figure S55. Writing in solid experiment. a) Slide before writing; b-e) four different patterns were drawn successively, using the same transparency slide. The UV lamp was on throughout the write/erase cycles. The pictures look blurred because of light reflection while taking the photos.

12 Two-photon Excitation Experiments

The luminescence band of **1-Z** and its isomerization to the *E*-form were observed upon irradiation with 800 nm light (i.e., NIR light), in both solution and solid film (Figure 4, Figures S56 and S57). Upon irradiation of **1-E** with light at 750 nm, spectral changes consistent with *E* to *Z* isomerization were also observed (Figures S58 and S59). The absorption cross-section of **1-Z** in toluene at 800 nm was measured to be 13.9 GM. This value, while relatively low,^{S12} is quite surprising considering the size of the chromophore, and is large enough to drive the photoisomerization process

Experimental setup: The excitation source for all the two-photon experiments was provided by a femtosecond Ti-sapphire oscillator (Tsunami, Spectra Physics) and regenerative amplifier laser system (BMI Alpha 1000) producing 430 mW, 100 fs pulses tunable in the 750-810 nm range at 1KHz repetition rate. Two-photon induced fluorescence of **1-Z** was recorded using an optical fiber coupled to a portable spectrometer (Ocean Optics USB-650). Data were acquired using 1s integration time. The sample was contained in a 1 cm quartz cuvette and excited at 800 nm. Two BG40 bandpass filters were placed in series before the detector to suppress the residual pump light. One-photon induced fluorescence was recorded for comparison using the same laser source and detection system. Excitation pulses at 400 nm were produced by second harmonic generation of the fundamental 800 nm laser radiation using a 2 mm thick BBO crystal. Fluorescence measurements were repeated in toluene and MeCN solutions. Emission spectra recorded upon one- and two-photon excitation appear identical in both solvents. The two-photon absorption cross section was determined following the fluorescence method as described in reference.^{S13} The excitation power for the measurement was set at 380 mW. Using a solution of Rhodamine B in methanol as standard ($\delta = 150 \times 10^{-50} \text{ cm}^4 \cdot \text{s}$),^{S14} the two-photon cross section of **1-Z** has been estimated using the following equation:

$$\delta_2 = \delta_1 \frac{F_2 \cdot \Phi_1 \cdot c_1}{F_1 \cdot \Phi_2 \cdot c_2} \quad \text{Eq. 10}$$

Here subscript 1 and 2 respectively refer to the sample and the standard, δ is the two-photon cross section, F is the integrated area of the two-photon induced fluorescence, Φ is the one-photon fluorescence quantum yield and c is the concentration. The fluorescence quantum yield of **1-Z** in toluene was estimated to be 0.016 using Rhodamine B as reference ($\Phi_1 = 0.71^{S15}$). The resulting two-photon cross section of **1-Z** in toluene is $13.9 \times 10^{-50} \text{ cm}^4 \cdot \text{s}$.

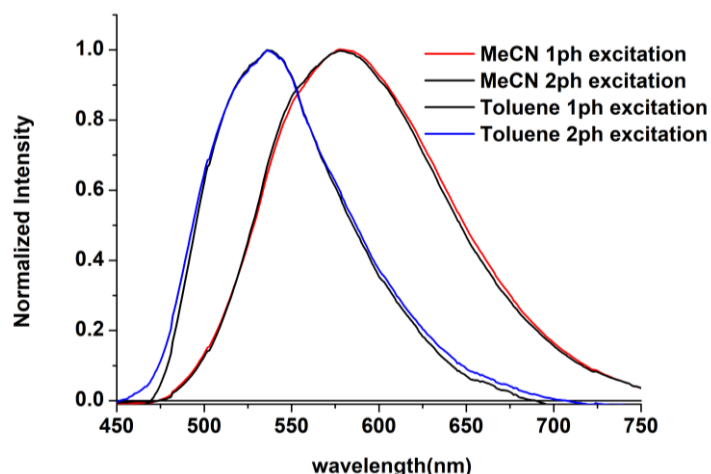


Figure S56. Fluorescence spectra of **1-Z** recorded in toluene ($3.8 \times 10^{-3} \text{ M}$; blue trace) and in acetonitrile ($3.7 \times 10^{-3} \text{ M}$; red trace) at room temperature upon two-photon excitation at 800 nm. The corresponding spectra obtained upon one-photon excitation at 400 nm are also shown (black lines).

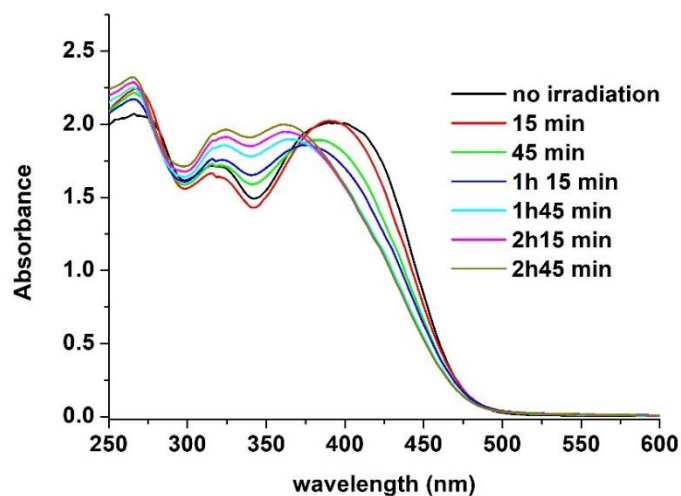


Figure S57. Absorption spectral changes observed upon two-photon irradiation of a solid film of **1-Z** at 800 nm.

2-Photon experiments on the 1-*E* form

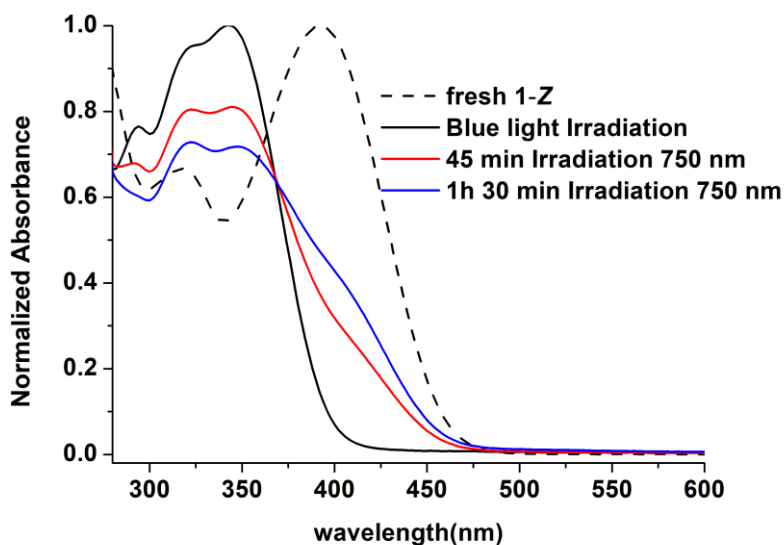


Figure S58. Absorption spectral changes observed upon two-photon irradiation at 750 nm of a toluene solution (5.6×10^{-5} M) containing predominantly the 1-*E* species. The sample was obtained by exhaustive irradiation of a solution of 1-*Z* (dashed line) with blue light provided by a LED source.

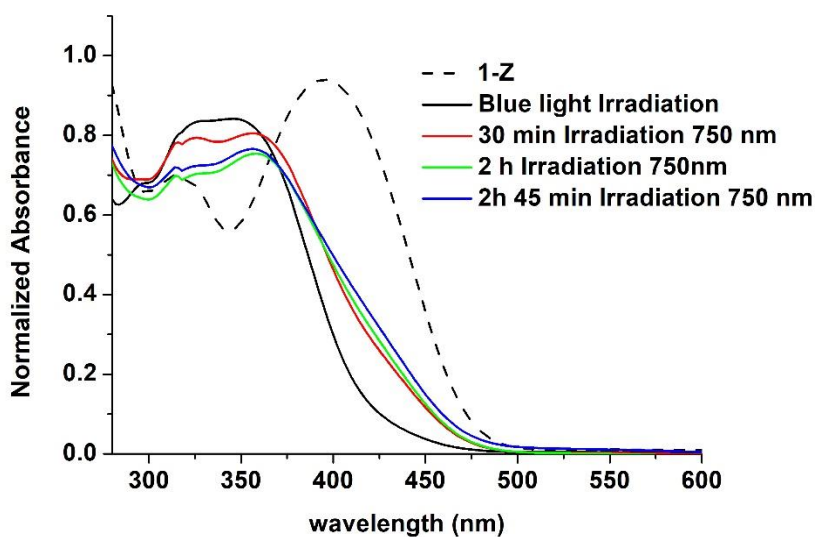


Figure S59. Absorption spectral changes observed upon two-photon irradiation at 750 nm of a drop casted solid film containing predominantly the 1-*E* species. The sample was obtained by exhaustive irradiation of a film of 1-*Z* (dashed line) with blue light provided by a LED source.

References

- S1 Barbara, B.; Couch, E. D.; Hardman-Baldwin, A. M.; Burtoloso, A. C.; Mattson, A. E. *Synthesis* **2016**, *48*, 677–686.
- S2 Huang, C-Y.; Bonasera, A.; Hristov, L.; Garmshausen, Y.; Schimdt, B. M.; Jacquemin, D.; Hecht, S. *J. Am. Chem. Soc.* **2017**, *139*, 15205–15211.
- S3 (a) Schonbrunn, E.; Eschenburg, S.; Luger, K.; Kabsch, W.; Amrhein, N. *Proc. Natl. Acad. Sci. USA* **2000**, *97*, 6345–6349; (b) Amdursky, N.; Kundu, P. K.; Ahrens, J.; Huppert, D.; Klajn, R. *ChemPlusChem* **2016**, *81*, 44–48.
- S4 (a) Weston, C. E.; Richardson, R. D.; Haycock, P. R.; White, A. J. P.; Fuchter, M. J. *J. Am. Chem. Soc.* **2014**, *136*, 11878–11881; (b) Qian, H.; Pramanik, S.; Aprahamian, I. *J. Am. Chem. Soc.* **2017**, *139*, 9140–9143.
- S5 (a) Kuhn, H. J.; Braslavsky, S. E.; Schmidt, R.; *Pure Appl. Chem.* **2004**, *76*, 2105–2146; (b) Bandara, H. M. D.; Friss, T. R.; Enriquez, M. M.; Isley, W.; Incarvito, C.; Frank, H. A.; Gascon, J.; Burdette, S. C. *J. Org. Chem.* **2010**, *75*, 4817–4827.
- S6 Demchenko, A. P.; Tang, K.-C.; Chou, P.-T. *Chem. Soc. Rev.* **2013**, *42*, 1379–1408.
- S7 Connors, K. A. *Chemical kinetics: the study of reaction rates in solution* VCH, New York, pp. 60–61, **1990**.
- S8 COSMO. V1.61 ed.; Bruker Analytical X-ray Systems: Madison, WI, **2009**, p Software for the CCD Detector Systems for Determining Data Collection Parameters.
- S9 SAINT-8.34A-2013 - Software for the Integration of CCD Detector System, Bruker Analytical X-ray Systems, Madison, WI, **2013**.
- S10 Sheldrick, G. M. *Acta Crystallogr.* **2008**, *A64*, 112–122.
- S11 Dolomanov, O. V.; Bourhis, L. J.; Gildea, R. J.; Howard, J. A. K.; Puschmann, H. *J. Appl. Crystallogr.* **2009**, *42*, 339–341.
- S12 Foucault, B.; Hermann, J. P. *Opt. Commun.* **1975**, *15*, 412–415.
- S13 Oulianov, D. A.; Tomov, I. V.; Dvornikov, A. S.; Rentzepis, P. M. *Opt. Comm.* **2001**, *191*, 235–243.
- S14 Xu, C.; Webb, W. W. *J. Opt. Soc. Am. B* **1996**, *13*, 481–491.
- S15 Crosby, G. A.; Demas, J. N. *J. Phys. Chem.* **1975**, *75*, 991–1024.